ORIGINAL ARTICLE

The refraction of shock pairs

L. F. Henderson · E. G. Puckett

Abstract We study shock refractions at the interface between two materials with convex equations of state involving only two shocks, which we refer to as shock pairs or shock pair systems. We present experimental and computational evidence for the existence of both regular and irregular shock pair systems in gases and develop a von Neumann type theory for regular systems that one can use to predict the angle of incidence at which a regular shock pair will occur. We show regular shock pair refractions obey the *Principle of Shock Reciprocity*; i.e., if the two materials are exchanged there is no effect on the polar diagram of the regular shock pair system, the angle between the two shocks in the pair or the streamline deflection angle. We also study regular and irregular shock pair systems in gases numerically and compare the numerical results with experimental data and our theory.

Communicated by R. Bonazza.

L. F. Henderson
School of Aerospace, Mechanical and Mechatronic Engineering,
University of Sydney, Sydney, NSW 2006, Australia
e-mail: leroy.henderson@bigpond.com

Present address:
L. F. Henderson
9A Point Road, Northwood, NSW 2066, Australia

E. G. Puckett (✉)
Department of Mathematics, University of California,
Davis, CA 95616, USA
e-mail: egpuckett@ucdavis.edu

1 Introduction

In this article, we study shock refractions involving only two shock waves at the interface between two materials with convex equations of state. We refer to these refractions as shock pairs or shock pair systems. We present experimental and computational evidence for the existence of both regular and irregular shock pair systems in gases and develop a von Neumann type theory for regular systems that one can use to predict the angle of incidence at which a regular shock pair will occur. We show regular shock pair refractions obey the *Principle of Shock Reciprocity*. In other words, if the two materials are exchanged there is no effect on the polar diagram of the regular shock pair system, the angle between the two shocks or the streamline deflection angle. Hence, there is no way to determine from the polar diagram of a regular shock pair which polar is the incident shock polar and which is the transmitted shock polar. In this case, we show how to use the concept of wave direction to distinguish between the incident and transmitted shocks by observing the regular shock pair system in the physical plane. We also study regular and irregular shock pair systems in gases numerically and compare the numerical results with experimental data and our theory.

In Sect. 1.1, we begin with a brief discussion of the refraction of an oblique shock wave at the interface between two media and wave impedance. The material in this section is a synopsis of the development and extensive discussion of the theory of wave impedance in [1]. Readers who are unfamiliar with this material are referred to [1] and the references there. We will need to refer to this material in the discussion that follows. In Sect. 1.2, we state the goals of this investigation and describe what is new and original about this work as compared to previous work in this area by the authors and others. Then, in Sect. 1.3 we conclude the introduction

with several paragraphs explaining how our presentation will proceed.

1.1 Shock refraction, shock polars, and wave impedance

In this section, we summarize the theory of wave impedance for the refraction of a plane shock wave striking a planar material interface at an oblique angle of incidence α_i. This material was developed and described in detail by Henderson in [1] and has been successfully used to study experiments and computations of oblique refraction in [2] and [3]. In the present article we prove that in the case of shock pair refraction the angle α_p at which the incident and transmitted shock impedances are equal, and other quantities derived from the equality of impedance condition, tend to the appropriate quantity in the acoustic limit. For example, we show that as the pressure jump across the incident and transmitted shocks tend to one $\alpha_p \rightarrow \alpha_p^*$, where α_p^* is the angle of intromission from acoustics [4]. We refer the interested reader to [1] for a more detailed account of the theory of wave impedance for oblique shock refraction.

In Sect. 1.1.2, we also briefly summarize the shock polar theory as it applies to our investigation of shock pairs.

1.1.1 Oblique shock refraction

Suppose a plane shock wave i is propagating with a velocity $\mathbf{U}_i$ in a material whose properties and state are known, and suppose also it enters another material with different properties, or state, which are also known, and which causes its velocity to change to $\mathbf{U}_t$. The shock will be said to refract whenever $\mathbf{U}_t$ differs in either magnitude or direction from $\mathbf{U}_i$. The shock will be called the incident shock i if it propagates in the incident material and the transmitted shock t if it propagates in the second or transmission material.

For simplicity we will assume the boundary between the two materials is a plane surface and that i encounters the boundary at some angle of incidence α_i. The angle of transmission α_t is related to the angle of incidence α_i by the refraction law,

$$\frac{U_i}{\sin \alpha_i} = \frac{U_t}{\sin \alpha_t}, \tag{1}$$

where $U_{i,t} \equiv |\mathbf{U}_{i,t}|$ denotes the magnitude of the vector $\mathbf{U}_{i,t}$; i.e., $U_{i,t}$ are the wave speeds for the i and t shocks, respectively, measured in the laboratory reference frame (Fig. 1).[1]

---

[1] In figures that contain a diagram of a shock wave system the incident shock i is always shown moving from right to left, since this is the direction i travels in the schlieren photographs of the experiments in [5, 6] and [7] (e.g., see Figs. 10, 11).
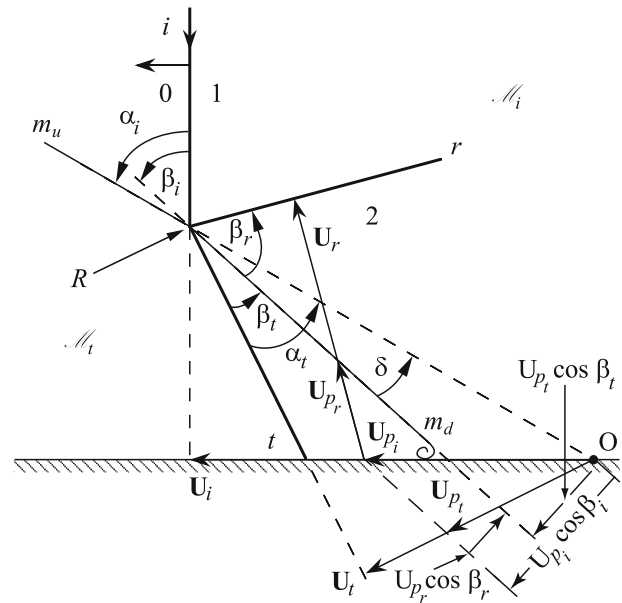
Fig. 1 Regular-refraction-with-a-shock-reflection (RRR). i, r, t, incident, reflected and transmitted shocks; $\mathbf{U}, \mathbf{U}_p$, velocity and piston vectors in the laboratory reference frame; $U_{p_{i,t,r}}$, signed magnitude of the piston vectors; $\mathscr{M}_i, \mathscr{M}_t$ incident and transmitted materials; m_u, m_d undisturbed and disturbed (deflected) material interface; α, β, wave angles with respect to the disturbed and undisturbed interfaces; δ, streamline deflection angle; R, refraction node; O, origin or 'corner'; Note $U_{p_i} \cos \beta_i + U_{p_r} \cos \beta_r = U_{p_t} \cos \beta_t$ [see (10)]

Here the term "laboratory frame" refers to the frame of reference in which the velocity $\mathbf{u}_0$ in the undisturbed medium ahead of the incident and transmitted shocks is $\mathbf{u}_0 = 0$. (More generally, one can define the laboratory frame to be the frame of reference in which the origin O (Fig. 1) is at rest with respect to $\mathbf{u}_0$.) The relative refractive index η is defined as

$$\eta \equiv \frac{U_i}{U_t} . \tag{2}$$

Combining (1) and (2) yields

$$\eta \equiv \frac{U_i}{U_t} = \frac{\sin \alpha_i}{\sin \alpha_t}, \tag{3}$$

from which it is concluded that the shock will be refracted (bent) by the materials if $\eta \neq 1$. A refraction is said to be slow–fast if $\eta < 1$ and fast–slow if $\eta > 1$.

Denote the speed of sound in the undisturbed initial material by a_{0i} and in the undisturbed transmission material by a_{0t}. The relative acoustic refractive index η_a [4] is defined by

$$\eta_a \equiv \frac{a_{0i}}{a_{0t}} . \tag{4}$$

Note that

$$\eta \equiv \frac{U_i}{U_t} \quad \rightarrow \quad \eta_a \equiv \frac{a_{0i}}{a_{0t}} \quad \text{as} \quad \xi_{i,t} \equiv \frac{P_{0i,t}}{P_{1i,t}} \quad \rightarrow \quad 1.$$

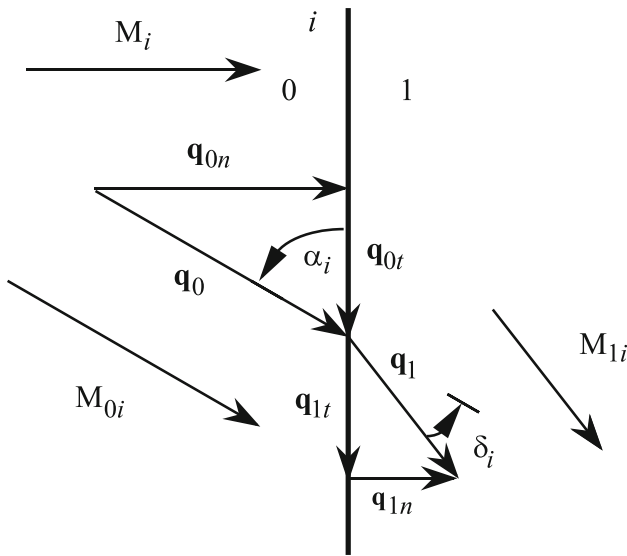In other words, $\eta \rightarrow \eta_a$ in the acoustic limit, $P_{1i,t} \rightarrow P_{0i,t}$.

Fig. 2 $\mathbf{q}_0$, $\mathbf{q}_1$, velocity of the flow upstream (resp. downstream) of, and relative to, the incident shock i; $\mathbf{q}_{0n}$, $\mathbf{q}_{1n}$, $\mathbf{q}_{0t}$ and $\mathbf{q}_{1t}$ normal and tangential components of the flow velocities $\mathbf{q}_0$ and $\mathbf{q}_1$ respectively; M_i, incident shock Mach number; M_{0i} and M_{1i}, undisturbed free stream Mach number upstream (resp. downstream) of, and relative to, i; α_i, angle of incidence or, equivalently, the angle between the upstream velocity $\mathbf{q}_0$ and i; δ_i, streamline deflection angle across i

1.1.2 Shock polars

Shock polars are used to describe steady-state shock waves and related flow states across steady oblique shocks. The equation of a shock polar is well known for the perfect gas equation of state (e.g., see p. 347 of [8] or p. 623 of [9]). For gamma-law gas equations of state one can find excellent discussions in such text books as Chapter IV of [10] or Chapter 9 of [11]. The derivation of the wave curve formulas for general equations of state have appeared in [12] and [13]. The derivations of these formulas are straightforward applications of the general theory for wave curves of hyperbolic systems as described in [14].

A derivation is presented here in outline for the shock polar associated with the incident shock i, which we refer to as the i shock polar. The equations for the t, n and s shock polars discussed later in this paper are derived in an analogous manner. Transforming now to coordinates at rest with respect to the refraction node R as shown in Fig. 2, let $\mathbf{q}_{0n} = -\mathbf{U}_i$ denote the normal component of the flow velocity $\mathbf{q}_0$ upstream of the incident shock i, measured in coordinates that are at rest with respect to i. Letting $q_{0n} = |\mathbf{q}_{0n}|$, the shock Mach number M_i is therefore

$$M_i \equiv \frac{U_i}{a_{0i}} = \frac{q_{0n}}{a_{0i}},$$

where a_{0i} is the speed of sound in the undisturbed flow ahead of the incident shock. The equation of the Rayleigh line follows from the continuity and momentum equations [15] as

$$q_{0n}^2 = P_0 V_0 \frac{P_1/P_0 - 1}{1 - V_1/V_0}.$$

The undisturbed free stream Mach number M_{0i}, which is constant everywhere on the shock polar, is found from

$$M_{0i}^2 = \frac{q_0^2}{a_{0i}^2} = \frac{M_i^2}{\sin^2 \alpha_i} = \frac{P_0 V_0}{a_{0i}^2 \sin^2 \alpha_i} \frac{P_1/P_0 - 1}{1 - V_1/V_0},$$

where $q_0 = |\mathbf{q}_0|$ denotes the speed of the flow which impinges on the shock, measured in coordinates that are at rest with respect to the refraction node R.

Now resolving the velocity vectors $\mathbf{q}_0$ and $\mathbf{q}_1$ upstream and downstream of an oblique shock into component vectors, $\mathbf{q}_{0n}$, $\mathbf{q}_{1n}$, $\mathbf{q}_{0t}$ and $\mathbf{q}_{1t}$ which are normal and tangential to the shock respectively (Fig. 2) and using the well-known fact that the tangential component of the velocity does not change across the shock ($\mathbf{q}_{0t} = \mathbf{q}_{1t}$), we have

$$\frac{q_{1n}}{q_{0n}} = \frac{V_1}{V_0} = \frac{\tan(\alpha_i - \delta_i)}{\tan \alpha_i}, \tag{5}$$

where δ_i is the streamline deflection angle across the incident shock (Fig. 2). Then from (5),

$$\tan \delta_i = \frac{(1 - V_1/V_0) \tan \alpha_i}{1 + (V_1/V_0) \tan^2 \alpha_i}. \tag{6}$$

The polar comprises a plot of $\ln(P_1/P_0)$ versus δ_i with M_{0i} held constant. In order to proceed any further, we need the equation of state for the material, or its equivalent, such as a set of tables. Then e_1 can be eliminated between it and the energy equation and a relation between P_1 and V_1 obtained. This in turn can be used to eliminate V_1 from (6). The polar is then defined once the initial state of the material and M_{0i} are given.

1.1.3 Wave impedance for oblique shock refraction

If $\alpha_i = 0$ there will, in general, be a reflected wave propagated back into the initial material as i passes into the transmission material. The reflection may either be a compression r or an expansion e. More precisely it will be a compression if the wave impedance $\mathcal{Z}$ increases $\mathcal{Z}_t > \mathcal{Z}_i$ and an expansion if $\mathcal{Z}$ decreases $\mathcal{Z}_t < \mathcal{Z}_i$, but there will be no reflection if there is no change in the impedance $\mathcal{Z}_t = \mathcal{Z}_i$. In this last case, the wave system consists only of two shocks.

The wave impedance for an arbitrary one-dimensional shock i is defined as in [1]

$$\mathcal{Z}_i \equiv \frac{P_1 - P_0}{U_{p_i}}, \tag{7}$$

where P is the pressure, the subscripts 0 and 1 refer to the conditions upstream and downstream of the shock, respectively,

and $U p_i$ is the (signed) speed of the piston associated with the i shock (Fig. 1). The piston velocity $\mathbf{U}_{p_i}$ can be thought of as the velocity of a moving boundary which generates the shock. In other words,

$$\mathbf{U}_{p_i} \equiv \mathbf{u}_1 - \mathbf{u}_0 \qquad (8)$$

where $\mathbf{u}_1$ is the velocity of the material downstream of the i shock. The vectors $\mathbf{U}_{p_i}$, $\mathbf{u}_0$, and $\mathbf{u}_1$ all are perpendicular to i and are defined in the laboratory frame. (However, it should be noted that the definition of $\mathbf{U}_{p_i}$ in (8) remains valid no matter what frame of reference one uses for $\mathbf{u}_0$ and $\mathbf{u}_1$.) If $\mathcal{Z}_i$ is now interpreted as the mass flux, then (7) is simply the momentum equation for the flow perpendicular to i and with magnitude $\mathcal{Z}_i$. It is sometimes convenient to consider $\mathcal{Z}_i$ as a vector $\boldsymbol{\mathcal{Z}}_i$ in the same direction as $\mathbf{U}_{p_i}$.

For an oblique shock (i.e., one for which $\alpha_i \neq 0$), the theory is simplified if we define an effective impedance $\mathbf{Z}_i$ by

$$\mathbf{Z}_i \equiv \frac{P_1 - P_0}{U_{p_i} \cos \beta_i} \frac{\mathbf{U}_{p_i}}{U_{p_i}}, \qquad (9)$$

where β_i is the disturbed angle of incidence; i.e., the angle that i makes with the disturbed (downstream) interface (Fig. 1). Note that the component of $\mathbf{Z}_i$ perpendicular to the disturbed interface reduces to $\mathcal{Z}_i$ as defined in (7). In what follows, we will usually use the effective impedance which we will simply refer to as "the impedance" unless stated otherwise.

For the r and t waves $\mathbf{Z}_r$ and $\mathbf{Z}_t$ are defined in a manner analogous to (9) with β_r, β_t, $\mathbf{U}_{p_r}$ and $\mathbf{U}_{p_t}$ defined as in Fig. 1. Note that since the component of the velocity downstream of the t-shock and normal to the (disturbed) material interface m_d must equal the component of the velocity downstream of the reflected r-shock that is normal to the interface, it follows that

$$U_{p_i} \cos \beta_i + U_{p_r} \cos \beta_r = U_{p_t} \cos \beta_t. \qquad (10)$$

This is depicted graphically in Fig. 1. Furthermore, in the absence of a reflected wave r, (10) reduces to

$$U_{p_i} \cos \beta_i = U_{p_t} \cos \beta_t.$$

The impedance $\mathcal{Z}_e$ of a one-dimensional expansion wave e may also be defined as in (7)

$$\mathcal{Z}_e \equiv \frac{P_2 - P_1}{U_{p_e}},$$

where P_1 and P_2 are the pressures upstream and downstream of the wave, respectively, U_{p_e} is the magnitude of the piston velocity $\mathbf{U}_{p_e} \equiv \mathbf{u}_2 - \mathbf{u}_1$ associated with the expansion and $\mathbf{u}_1$ and $\mathbf{u}_2$ are the velocities of the medium upstream and downstream of the wave. Note that $\mathbf{U}_{p_e}$ is the velocity of a piston that is withdrawing in the direction opposite that of the
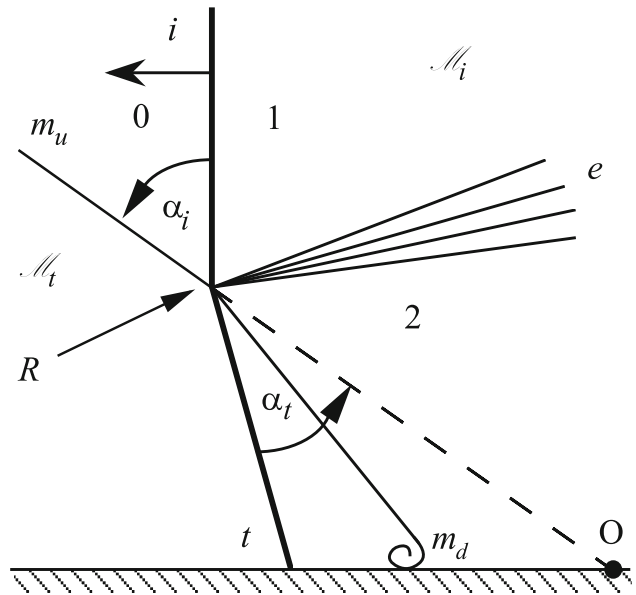
Fig. 3 Regular-refraction-with-a-reflected-centered-expansion wave (RRE)

wave propagation. The definition of the effective impedance (vector) $\mathbf{Z}_e$ for an expansion wave in two dimensions is more difficult, since an expansion of say, the Prandtl–Meyer type, is not a single plane surface but a fan of such surfaces (Fig. 3). However, its magnitude Z_e can be defined as

$$Z_e \equiv \frac{P_2 - P_1}{\int d(U_{p_j} \cos \beta_j)}$$

where U_{p_j} denotes the magnitude of the piston velocity $\mathbf{U}_{p_j}$ associated with the "jth wave" in the expansion fan and β_j denotes the angle this wave makes with the disturbed gas interface [1]. This may be rewritten in a more computationally useful form as

$$Z_e = \frac{P_2 - P_1}{(\mathbf{u}_2 - \mathbf{u}_1) \cdot \mathbf{n}}$$

where $\mathbf{n}$ is the unit vector normal to the disturbed gas interface.

1.2 The goals of this investigation

A refracting wave system is said to be regular when all of its waves meet at a single point, or node, R on the material interface and are all locally straight at that point as illustrated in Figs. 1 and 2. If the flow fields in a neighborhood of R and between the waves and the interface are uniform, then a particular field will have a constant particle velocity $\mathbf{u}$ and constant thermodynamic state (S, V), where S and V are the specific entropy and specific volume, respectively. The refraction is said to be irregular when there is at least one curved wave at R and at least one non-uniform flow field in a
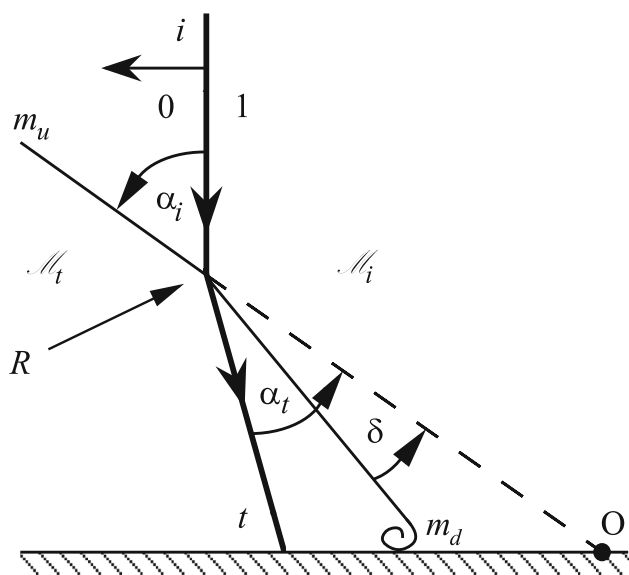
Fig. 4 Regular-shock-pair refraction (RSP) $(i - t)$ with $M_{1i} > 1$ and $M_{1t} > 1$; note that the angle α_t is measured with respect to the undisturbed material interface m_u downstream of the refraction node R

neighborhood of R. It is well known that the refraction will be regular when α_i is sufficiently small but that otherwise it will be irregular [1,16,17] and [18].

The simplest experiments on shock wave refraction at the interface between two gases are conducted in the self-similar configuration, a diagram of which is shown in Fig. 1. These experiments are typically done with the gases initially separated by a very delicate membrane, as for example in the experiments described in [5–7] and [17]. In these experiments the authors' used both weak and strong shocks and photographed both regular and irregular wave systems. They observed a number of irregular systems, including anomalous refractions (AR) [5] and [17], Mach-reflection–refractions (MRR) [5,17], and [17], and PreCursor-Mach-refractions (PCMR) [6,7] and [2].

An illustration of a regular-refraction-with-a-reflected-expansion (RRE) appears in Fig. 3. In [17] it was shown that it is also possible for the reflected wave to be a shock; i.e., a regular-refraction-with-a-shock-reflection (RRR) as shown in Fig. 1. The i and t shocks form a regular shock pair at the transition RRE $\rightleftharpoons$ RRR where the reflected wave degenerates into a Mach line. An illustration of this system appears in Fig. 4.

Examination of the irregular shock refraction systems in the references cited above reveals that some irregular systems have shock pairs as part of the refraction; for example, see the diagram of an MRR in Fig. 8. The schlieren photograph of it in Figs. 10 and 11 show the Mach shock n refracting into the transmitted shock t. Similar refracting pairs occur in some PCMR systems. For example, see the diagrams in Figs.

12 and 13, which show the transmitted shock t refracting into the side shock s.

The goals of this paper are as follows. The principle goal of this paper is to develop a theory for the refraction of regular shock pairs. The basis of this theory is a formula for predicting the angle of incidence $\alpha_i = \alpha_p$ at which a regular shock pair refraction will occur. We verify the validity of this formula with our numerical computations. This is an important but perhaps easily overlooked result. We have found that the ability to predict α_p, in combination with other ideas, has been useful in analyzing more general irregular refractions such as anomalous refraction (e.g., see [3]).

Second, we classify shock pair refractions by presenting theoretical, experimental and numerical evidence to show they can occur in all four of the possible configurations; i.e., the flow downstream of either shock in the pair can be supersonic or subsonic with respect to that shock. Besides the regular refraction that occurs at the transition RRE $\rightleftharpoons$ RRR, in which the flow is supersonic downstream of both the i and t shocks, we present an example of a shock pair in a fast–slow gas combination in which the flow is supersonic downstream of one member of the pair and subsonic downstream of the other and another example of a shock pair in a slow–fast gas combination in which the flow is subsonic downstream of both members of the shock pair. Both of these examples are in agreement with shock polar analysis and our numerical computations and are supported by photographs of the refraction (either in Figs. 10, 11 or in cited references).

We also present theoretical, experimental and numerical data from a sequence of shock refractions with a fixed gas combination (Air/SF_6) and inverse incident shock strength $\xi_i \equiv P_0/P_1$ over an interval (α_l, α_r) of angles of incidence α_i in which each refraction contains a shock pair. Using this data we demonstrate the shock pairs are irregular in all of the refractions but at the end point of the sequence, thereby confirming the existence of irregular shock pairs. We then argue that the irregular shock pairs do not obey the assumptions underlying our theory of regular shock pairs. In addition, this example shows a regular $i - t$ shock pair of 'subsonic-supersonic' type (i.e., in which the flow downstream of the i-shock is subsonic and the flow downstream of the t-shock is supersonic) can exist as the endpoint, or boundary, of a continuum of irregular refractions containing irregular shock pairs.

There is very little discussion in the literature about the existence of shock pair refractions. The only reference we could find was in Glimm et al. [19]. They considered it during their studies of two-dimensional Riemann problems and called it a "transmission node". To the best of our knowledge the work described in this article is new and original. It follows naturally from the previous work of the authors in [1] and [2]. In addition, in [3] we use the formula that we derive in the present article for predicting the angle α_p

at which a regular shock pair occurs, to study refractions in which the flow downstream of the incident shock is subsonic at the interface in coordinates with respect to the refraction node R. For example, in [3] we use this formula in combination with other ideas to predict the angle α_p of the regular shock pair that forms the boundary of one side of a continuum of refraction systems (parameterized by α_i with the gas combination and shock strength ξ_i fixed) found by Abdel-Fattah and Henderson in [5], in which the incident shock i is partly overrun by upstream moving compressions arising in its rear that locally strengthen it and cause it to curve forward in a neighborhood of R. In other words, this continuum of refraction systems lies in the interval (α'_i, α_p) for some angle of incidence α'_i. Furthermore, on the other side of this boundary (i.e., in the interval (α_p, α''_i) for some α''_i) the incident shock i is partly overrun by upstream moving expansion waves that locally weaken it and cause it to curve backward in a neighborhood of R.

In summary, while we believe shock pair systems are of interest in their own right, we have also found the regular shock pair theory presented in this article to be quite useful in our analysis of certain irregular refraction systems. We plan to present additional work along these lines in a companion article at a later date.

1.3 An overview of this article

In Sect. 2.1 we list the assumptions we have made concerning the equations of state of each material in a shock pair refraction. Then, in Sect. 2.2 we review in detail the assumptions that underly our definition of a regular shock pair. In Sect. 2.3 we present an equation for predicting the angle of incidence $\alpha_i = \alpha_p$ at which a regular shock pair will occur. It is a quadratic equation for $x = \sin^2 \alpha_p$. This greatly simplifies the calculation of α_p. The coefficients of this quadratic equation depend on the thermodynamic properties of the two materials. Thus, the equation of state of each material must be given in order to solve for α_p, which can then be compared with computations and experiments.

Next, in Sect. 3 we classify shock pair refractions in terms of whether the flow is supersonic downstream of both shocks, supersonic downstream of one and subsonic downstream of the other or subsonic downstream of both. In Sect. 3.1–Sect. 3.3 we use shock polar diagrams to illustrate each of these cases. In order to justify the use of shock polars in the cases where the shock pair is irregular and unsteady, in Sect. 3.4 we argue that these latter systems occur locally as a self-similar system in a coordinate frame in which the origin is at the refraction node R, and therefore they are 'pseudo-steady'.

In Sect. 4 we introduce the *Principle of Shock Reciprocity*, which states that, for a regular shock pair, if the two materials are exchanged there is no effect on the polar diagram

for the regular shock pair system the angle between the two shocks in the system or on the streamline deflection angle. In order to determine which of the two shocks in the pair is the incident shock and which is the transmitted shock we use the concept of wave direction, which we review in Sect. 4.1. Then, in Sect. 4.2 we formally define the *Principle of Shock Reciprocity* and describe how one can use the wave direction to differentiate between the incident and transmitted shocks in the physical plane.

In Sect. 5 we briefly discuss the experiments from which we obtained our experimental data and the schlieren photograph shown in Figs. 10 and 11. In Sect. 6.1 we describe the numerical method we used to obtain our computational results and in Sect. 6.2 we list the numerical parameters we used in our computations, such as the size of the computational domain, grid refinement and other details relevant to these computations.

In Sect. 7 we present experimental and numerical evidence in perfect gases for the existence of regular and irregular shock pair refractions. In Sect. 7.1 we compare experimental data from a sequence of experiments in the Air/SF_6 gas combination with $\xi_i = 0.25$ over an interval (α_l, α_r) of angles of incidence α_i with data obtained from our computations and data calculated from the regular shock pair theory under the assumption that each of the shock pairs in the sequence is regular. Upon comparison we find the regular shock pair theory agrees with the experimental and numerical data only at the right-hand α_r endpoint of the sequence. We conclude all of shock pairs in the sequence but the last are irregular. Finally, in Sect. 7.2 we present contour plots from some of our computations of regular and irregular shock pairs in three different gas combinations. These computational results support the analysis presented in the previous sections, demonstrate the wide range of parameter space over which shock pairs are found, and illustrate the utility of understanding shock pair refraction as a separate phenomenon in its own right. We finish with a discussion of our conclusions in Sect. 8.

2 Shock pair refractions

By definition, a shock pair refraction consists of only two shocks i and t, say. Since there is no reflected wave, the (effective) wave impedances are equal in magnitude,

$$Z_i \equiv \frac{P_{1i} - P_0}{U_{p_i} \cos \beta_i} = \frac{P_{1t} - P_0}{U_{p_t} \cos \beta_t} \equiv Z_t. \tag{11}$$

In addition, we assume the von Neumann 'jump' or 'boundary' conditions apply everywhere along the material interface; i.e., there is no change in pressure or in streamline direction across the interface (e.g., see [20]).

2.1 Assumptions on the equations of state of the materials

We assume that the equation of state for each material has the form $P = P(V, T)$ where V is the specific volume and T is the temperature. We also assume that each equation of state obeys the general convexity condition (e.g., see [21]),

$$\left(\frac{\partial^2 P}{\partial V^2}\right)_S > 0, \tag{12}$$

or equivalently,

$$\mathcal{G} \equiv \frac{V^3}{2a^2}\left(\frac{\partial^2 P}{\partial V^2}\right)_S > 0,$$

where

$$a^2 = -V^2\left(\frac{\partial P}{\partial V}\right)_S$$

is the speed of sound squared and $\mathcal{G}$ is the non-dimensional form of the derivative in (12); i.e., the fundamental derivative (e.g., see [11]). The condition in (12) is obeyed by nearly all materials that are in a single phase (e.g., see [22]), although it can fail near a phase boundary (e.g., see [21,23] and [24]).

2.2 The regular refraction of a shock pair

Suppose the flow fields are uniform in a neighborhood of the shock node R as shown in Fig. 4. In this case the shock pair is, by definition, a regular refraction. If the flow is not uniform in a neighborhood of R, then the system is an irregular refraction. For regular refraction the pressure jumps across the shocks are equal,

$$P_{1i} - P_0 = P_{1t} - P_0, \tag{13}$$

and hence (11) implies

$$U_{p_i} \cos \beta_i = U_{p_t} \cos \beta_t. \tag{14}$$

The refraction law (1) provides an extra equation and also a relation between the flow Mach numbers M_{0i} and M_{0t} of the i and t shocks

$$a_{0i} M_{0i} = a_{0t} M_{0t}, \tag{15}$$

where (1) is for the laboratory frame and (15) is for the frame at rest with respect to the refraction node R. In particular, the flow Mach numbers M_{0i} and M_{0t} are always measured with respect to R.

These equations, together with the equations of state for the materials and the Rankine–Hugoniot equations are a complete formulation of the regular two-shock refraction problem. Specifically, a solution is defined on the parameter set $(a_{0i}, a_{0t}, \xi_i, \alpha_i)$, where the parameter $\xi_i \equiv (P_0/P_1)_i$ is the inverse shock strength of the incident shock i. More compactly, one can write $(\eta_a, \xi_i, \alpha_i)$. Thus, the parameter space for the solution is a subset of $\Omega = [0, \infty] \times [0, 1] \times [0, \pi/2]$.
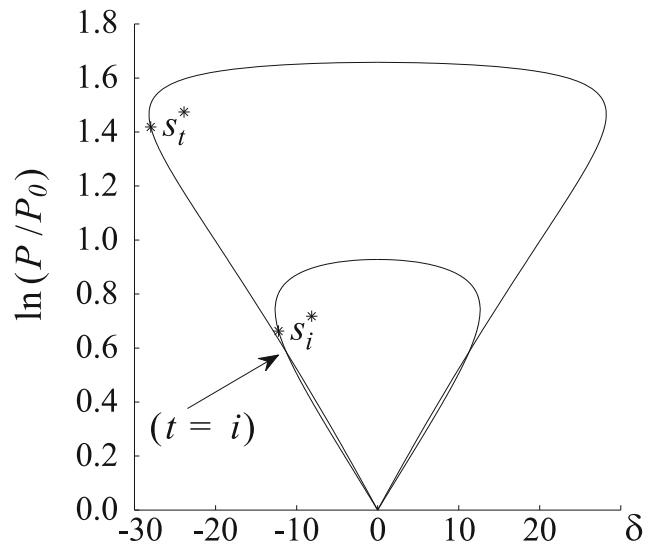

Fig. 5 Shock polar diagram for the Air/CO_2 gas combination with $M_{0i} = 1.5204$ and $M_{0t} = 1.9538$ corresponding to an $(i - t)$ pair such as the one in Fig. 4; $t = i$, intersection of the i and t polars; s_i^*, s_t^*, sonic points on the i and t polars
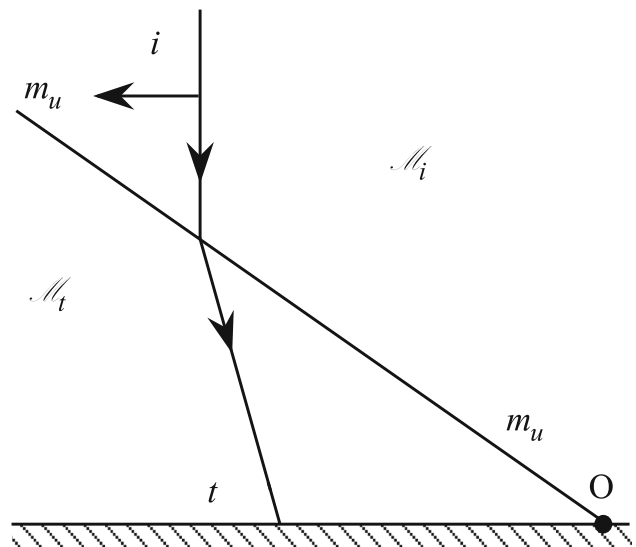

Fig. 6 Regular refraction of an acoustic wave pair $(i - t)$. This wave pair is the acoustic limit of the RSP shown in Fig. 4. In other words, it is the limit as $\xi_i \equiv P_0/P_1 \to 1$ of the RSP in Fig. 4

A diagram of a regular shock pair refraction is shown in Fig. 4. Each of the i and t shocks maps into its own polar in the $(\delta, \ln(P_1/P_0))$ plane. However, since there is no reflected wave, each shock must have the same polar coordinates, which are denoted by $(t = i)$ in Fig. 5. For $\xi_i \equiv P_1/P_0 = 1$ (Figs. 6, 7), the i and t shocks are reduced to acoustic degeneracies, which in the present context are regarded as trivial. For $P_1/P_0 > 1$, the shock pair possibilities are as illustrated in Figs. 4, 5, 6, 7, 8, 9, 10, 11, 12 and 13. They are classified according as to whether the flow Mach numbers M_{1i} and
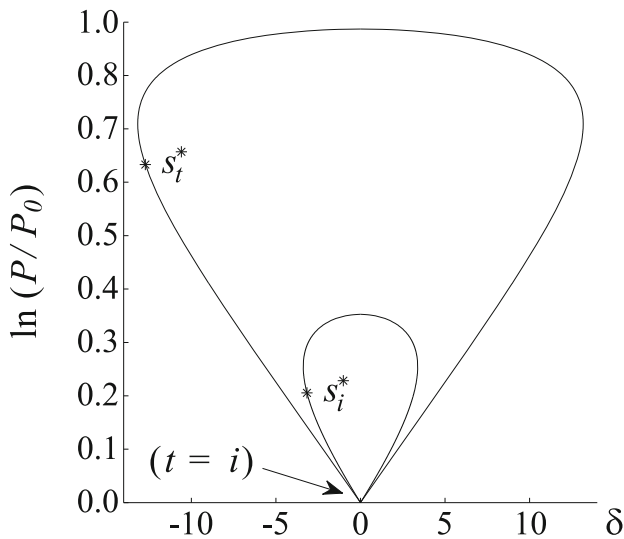
Fig. 7 Shock polar diagram for the CH_4/CO_2 gas combination with $M_{0i} = 1.172$ and $M_{0t} = 1.506$ corresponding to an $(i - t)$ pair such as the one in Fig. 6; $t = i$, intersection of the i and t polars; s_i^*, s_t^*, sonic points on the i and t polars
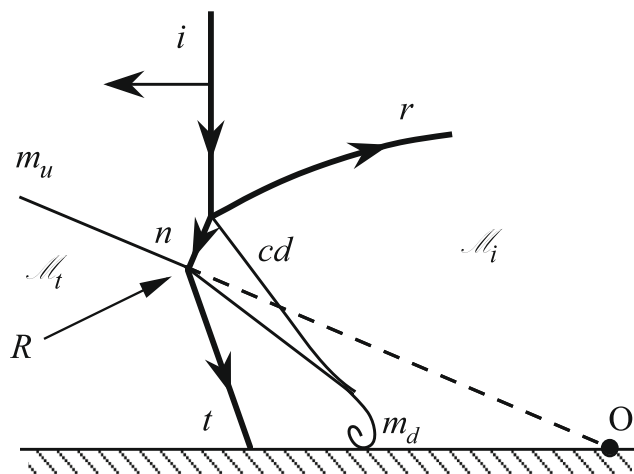

Fig. 8 Mach-reflection–refraction (MRR) containing an irregular-shock-pair refraction (ISP) $(n - t)$ with $M_{1n} < 1$ and $M_{1t} > 1$; n, normal or Mach shock; cd, contact discontinuity; this diagram corresponds to the schlieren photograph shown in Fig. 10

M_{1t} downstream of i and t, and relative to them, are either supersonic or subsonic.

2.3 A formula for predicting a regular shock pair

Suppose we are given two materials, an incident material $\mathscr{M}_i$ and a transmission material $\mathscr{M}_t$, together with their equations of state and the inverse incident shock strength $\xi_i \equiv (P_0/P_1)_i$. We would like to predict the angle of incidence $\alpha_i = \alpha_p$ at which a regular shock pair refraction will occur. This is equivalent to obtaining an expression for the polar intersection point $t = i$ shown in Fig. 5.
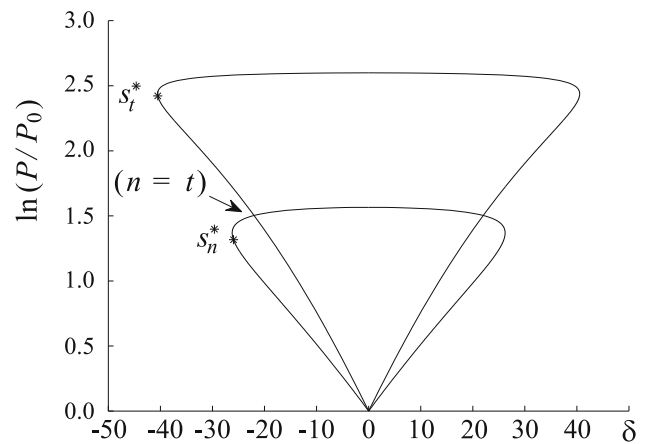
Fig. 9 Shock polar diagram for the CO_2/CH_4 gas combination with $M_{0n} = 3.473$ and $M_{0t} = 2.085$ corresponding to an $(n - t)$ pair such as the one in Fig. 8; $n = t$, intersection of the n and t polars; s_n^*, s_t^*, sonic points on the n and t polars
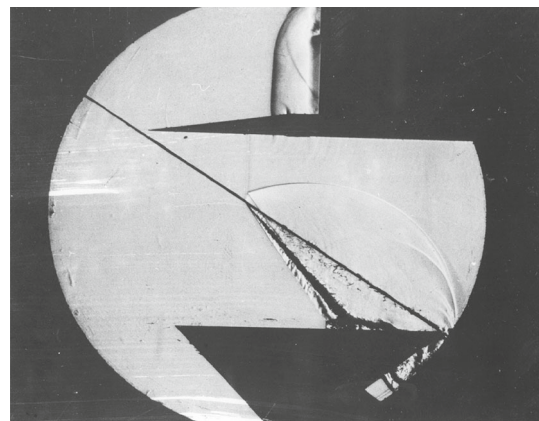

Fig. 10 schlieren photograph for the Air/SF_6 gas combination with $\xi_i = 0.25$ and $\alpha_i = 58°$; note that the i, n and t shocks are all traveling from *right* to *left* as shown in the diagram in Fig. 8

One can solve this problem using equations (1) and (14) together with the Rankine–Hugoniot equations and the equation of state for each material. After a tedious calculation, during which a number of variables such as α_t, β_i and β_t are eliminated, one can obtain an equation for $\alpha_i = \alpha_p$ in terms of $\eta \equiv U_i/U_t$, the undisturbed material specific volume ratio V_{0t}/V_{0i}, and the shock strength parameters $(V_1/V_0)_i$ and $(V_1/V_0)_t$, which are the specific volume ratios across the i and t shocks, respectively. If we let $x \equiv \sin^2 \alpha_p$, then x satisfies the following quadratic equation:

$$A_2 x^2 + A_1 x + A_0 = 0, \tag{16}$$

with coefficients

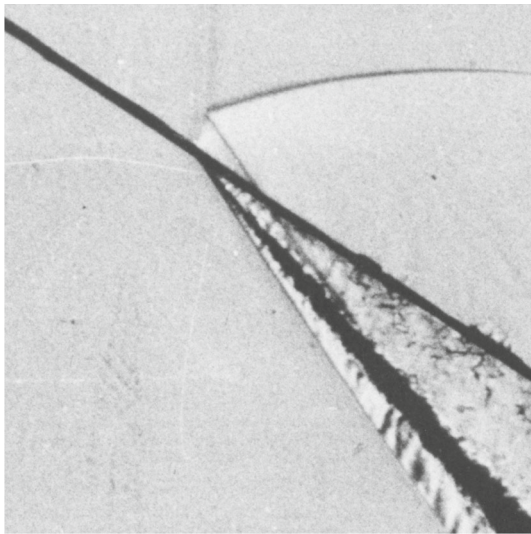$$A_0 \equiv 1 - \eta^2 \left(\frac{V_{0t}}{V_{0i}}\right)^2, \tag{17a}$$

Fig. 11 Enlargement of Fig. 10 about the refraction node R in which the contact discontinuity cd and the Mach shock n are clearly visible; note the thickness of the disturbed gas interface
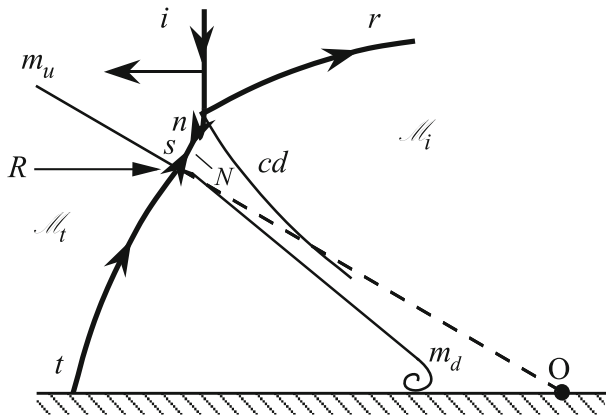

Fig. 12 PreCursor-Mach-refraction (PCMR) containing an irregular-shock-pair (ISP) $(t-s)$ with $M_{1t} < 1$ and $M_{1s} < 1$; s, side shock; n, normal or Mach shock; cd, contact discontinuity; N, point at which s and n shocks meet; (after the experiments in [17], Figs. 14 and 18)

$$A_1 \equiv -\left\{ \eta^{-2}\left[1-\left(\frac{V_1}{V_0}\right)_t^2\right] - \eta^2\left(\frac{V_{0t}}{V_{0i}}\right)^2 \right.$$
$$\left. \times \left[1-\left(\frac{V_1}{V_0}\right)_i^2\right] + \left[1-\left(\frac{V_{0t}}{V_{0i}}\right)^2\right] \right\}, \quad (17b)$$

$$A_2 \equiv \eta^{-2}\left[1-\left(\frac{V_1}{V_0}\right)_t^2\right] - \left(\frac{V_{0t}}{V_{0i}}\right)^2\left[1-\left(\frac{V_1}{V_0}\right)_i^2\right]. \quad (17c)$$

In order to proceed further, the equations of state of the materials must be known. Let B_0, B_1 and B_2 denote the coefficients of the quadratic polynomial in (16) when the two materials are perfect gases that obey the equation of state for an ideal gas. Then (17) becomes
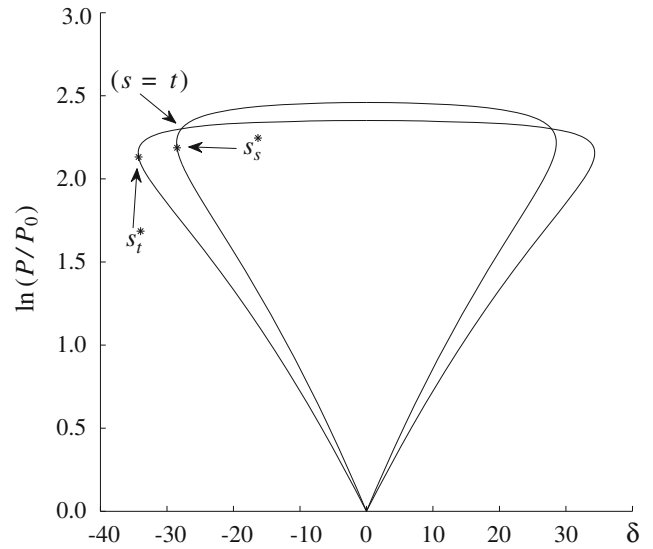

Fig. 13 Shock polar diagram for the Ar/O$_2$ gas combination with $M_{0t} = 3.091$ and $M_{0s} = 2.953$ corresponding to a $(t-s)$ pair such as the one in Fig. 12; $s = t$, intersection of the s and t polars; s_s^*, s_t^*, sonic points on the s and t polars

$$B_0 = 1 - \frac{\mu_i}{\mu_t}\gamma_i(\gamma_i+1)M_i^2[\gamma_i(\gamma_t+1)M_i^2+\gamma_t-\gamma_i], \quad (18a)$$

$$B_1 = -\left\{1-\left(\frac{\mu_i}{\mu_t}\right)^2 \right.$$
$$\left. +4\frac{\mu_i}{\mu_t}\frac{(\gamma_t-\gamma_i)}{\gamma_i+1}\frac{(M_i^2-1)(1+\gamma_i M_i^2)}{M_i^2[\gamma_i(\gamma_t+1)M_i^2+\gamma_t-\gamma_i]}\right\}, \quad (18b)$$

$$B_2 = 4\frac{\mu_i}{\mu_t}\frac{(M_i^2-1)(1+\gamma_i M_i^2)}{(\gamma_i+1)^2 M_i^4[\gamma_i(\gamma_t+1)M_i^2+\gamma_t-\gamma_i]}$$
$$\cdot\left\{\gamma_t(\gamma_i+1)M_i^2-\frac{\mu_i}{\mu_t}[\gamma_i(\gamma_t+1)M_i^2+\gamma_t-\gamma_i]\right\}, \quad (18c)$$

where μ_i, μ_t are the molecular weights and γ_i, γ_t are the ratio of specific heats of the incident and transmitted gases respectively.

In the acoustic limit $V_1/V_0 \to 1$, or equivalently, $M_i \to 1$, then (16) with (17) or with (18) gives exactly the same result. That is, the acoustic limit is independent of the equations of state. Thus,

$$\sin^2\alpha_p^* = \frac{1-(r_i/r_t)^2}{1-(V_{0t}/V_{0i})^2} \quad (19)$$

where $r_{i,t} \equiv \rho_{0i,t}a_{0i,t} = a_{0i,t}/V_{0i,t}$ is the acoustic impedance of the incident and transmission materials and $\rho_{i,t} = 1/V_{i,t}$ is their density. Equation (19) is exactly the same as a well-known one in acoustics in which α_p^* is called the angle of intromission (e.g., see [4], p. 158). As noted in [4], this angle can exist only under two circumstances:

1. $r_i < r_t$ and $V_{0i} < V_{0t}$,
2. $r_i > r_t$ and $V_{0i} > V_{0t}$.

Given the system parameters $(\eta_a, \xi_i, \alpha_i)$ defined in Sect. 2.2, equation (16) can be solved for α_p, giving two values for α_p. The geometry of the system boundary will determine which solution appears for the corresponding RSP. Only one solution can occur for a given set of parameters, so it follows more generally that the RSP is not robust; it occurs as the separating condition between either a regular, such as RRR $\rightleftharpoons$ RRE, or an irregular system, such as RRR $\rightleftharpoons$ PCMR.

3 The classification of shock pair refractions

3.1 The all-supersonic case $M_{1i} > 1$ and $M_{1t} > 1$

A diagram of the all-supersonic case is shown in Fig. 4 and two shock polars illustrating this case are shown in Fig. 5. This case has been discussed in previous papers (e.g., [2]). It lies on the transition between a shock refraction with a reflected shock (RRR) and one with a reflected expansion (RRE). In other words, the shock pair occurs at the transition RRR $\rightleftharpoons$ RRE, where the reflected wave (r or e) degenerates to a Mach line and equations (11) to (15) are satisfied. A computation of this transition for the CO_2/CH_4 slow–fast gas combination is shown in Fig. 4b of [2] and for the Air/CO_2 fast–slow gas combination in Fig. 3c of [3].

The flow fields are everywhere supersonic and uniform in a neighborhood of the refraction node R, so this system is a regular refraction. However, any infinitesimal variation in one or more of the system parameters $(\eta_a, \xi_i, \alpha_i)$ will, in general, cause the shock pair system to change into one of the adjacent two wave systems, RRR or RRE. In this respect it may be noted that the polar for the reflected shock in an RRR and the characteristic for the reflected expansion in an RRE form non-trivial polar intersections once i moves away from the intersection point of the M_{0i} and M_{0t} polars.

In our earlier paper [2] we showed that RRR and RRE occupy a subspace of finite volume in the parameter space Ω, while the wave pair refraction lies only on the boundary between these two subspaces. Therefore, it occupies zero volume. Furthermore, the subsets $\Omega_R \subset \Omega$ and $\Omega_E \subset \Omega$ occupied by RRR and RRE are open subsets of Ω in the sense that about each point $(\eta_a, \xi_i, \alpha_i) \in \Omega_R$ or $(\eta_a, \xi_i, \alpha_i) \in \Omega_E$ one can construct an open neighborhood contained entirely within Ω_R or Ω_E. Therefore, an RRR or an RRE will survive any infinitesimal perturbation of its state. Such systems are called generic or robust [19]. On the other hand, since the set of all shock pair refractions satisfying $M_{1i} > 1$ and $M_{1t} > 1$ lies on the boundary between Ω_R and Ω_E, every open neighborhood of a point in this set will also contain points in Ω_R and Ω_E. Hence, this shock pair refraction is not generic or robust. Physically, the shock pair can only exist fleetingly under variations of the system parameters.

3.2 The mixed supersonic–subsonic case $M_{1i} > 1$ and $M_{1t} < 1$ or $M_{1i} < 1$ and $M_{1t} > 1$

The mixed shock pair can occur in at least two situations, either as an $i - t$ pair similar to Figs. 4 and 5 except that now $M_{1i} < 1$ with a corresponding change in the polar intersection (e.g., see Figs. 23, 24), or as part of a MRR in which the Mach shock n refracts to produce the t shock with $M_{1n} < 1$ and $M_{1t} > 1$ as shown in the diagram in Fig. 8. Two shock polars illustrating this latter case are shown in Fig. 9. Since $M_{1n} < 1$ there can be no reflected wave at the node R on the interface. Consequently, there is no reflected shock polar or isentrope to represent a reflected shock or expansion wave. Furthermore, so long as $M_{1n} < 1$ this conclusion will still apply, and the two-shock refraction will therefore survive infinitesimal variations in the system parameters. Thus, in this case it is generic. Systems of this type were detected in the experiments of Abd-el-Fattah and Henderson [5] with shocks being refracted by the Air/SF_6 gas combination. A schlieren photograph from [5] for this gas combination for $\xi_i = 0.25$ and $\alpha_i = 58°$ is shown in Figs. 10 and 11.[2]

3.3 The all subsonic case $M_{1i} < 1$ and $M_{1t} < 1$

A diagram of a shock pair $t - s$ with $M_{0t} < 1$ and $M_{0s} < 1$ is illustrated in Fig. 11. Two shock polars illustrating this case are shown in Fig. 13. Once again there can be no reflected wave from the interface. The t and s polars intersect on the subsonic parts of both polars. By arguments similar to the previous case the $t - s$ pair is generic. The appearance of a $t - s$ shock pair in a PreCursor-Mach-refraction (PCMR) is discussed in Sect. 7.2.2. It has been detected during experiments with the Air/CH_4 gas combination [17] (see Plate 6, Fig. 14c and Plate 12, Fig. 18).

3.4 The shock polar analysis of irregular shock pairs

Regular refractions can be regarded as solutions to Riemann problems for steady supersonic flows, and as such can be interpreted using shock polars. Irregular refractions on the other hand are not steady, but only pseudo-steady or self-similar (scale invariant) as solutions to two-dimensional Riemann problems for time dependent flows.

---

[2] In the schlieren photograph in Figs. 10 and 11 the feature that appears as a straight black line inclined at an angle of $\alpha_i = 58°$ to the vertical is the edge of the wire frame used to hold the thin polymer membrane that initially separated the two gases. See [6] for details of the experimental setup.

So for example, consider the MRR system in Figs 8, 9, 10 and 11, where the n-shock refracts into the t-shock. If one assumes the Mach node (i.e., the triple point) follows a straight path beginning at O, then the von Neumann theory agrees quite well with experiment. The n-shock has its end points on that path and on the plane surface at the $n-t$ node R on the gas interface. Consequently, this shock is self-similar, both in the coordinate system with the origin at the Mach node (triple point) and in the coordinate system with the origin at R. In either frame of reference it can be treated as pseudo-stationary. Similarly, in the coordinate frame with the origin at R the t-shock is also self-similar in a neighborhood of R. Thus, the flow in a neighborhood of R is pseudo-stationary in the coordinate frame centered on R, and one can use shock polars such as the one in Fig. 9 to analyze the MRR systems as we have done in Sect. 3.2.

There are numerous schlieren photos of PCMR systems in [2,7] and [17] that contain $t-s$ wave pairs. They have been extensively studied numerically in [2]. The photos in [7] and [2] clearly show the systems are self-similar in the coordinate systems mentioned above. One can similarly justify the use of shock polars such as the one shown in Fig. 13 to analyze PCMR systems as we have done in Sect. 3.3 by noting that the flow is pseudo-stationary in the coordinate frame with its origin at the point R shown in Fig. 11.

4 The principle of shock reciprocity

Each wave in a shock pair such as $i-t$, $n-t$, or $t-s$ maps into the same polar intersection point ($t=i$, $t=n$, or $s=t$) as shown in Figs. 5, 9, 13, so it is impossible to determine from the polar plane which is the incident and which is the transmitted shock. This suggests the *Principle of Shock Reciprocity*, similar to the one for acoustic reciprocity [4]. Namely, it makes no difference to the refraction if a shock passes from the first material into the second or vice versa. Although this is correct for the polar plane some difficulty can arise in the physical plane. In order to understand it we review an idea used by von Neumann, and also by Glimm et al. in [19], called wave direction.

4.1 The wave direction

Referring now to Fig. 2 one can resolve the flow vector $\mathbf{q}_0 = \mathbf{q}_{0n} + \mathbf{q}_{0t}$ upstream of, and in coordinates relative to, the i shock (say) into component vectors $\mathbf{q}_{0n}$ and $\mathbf{q}_{0t}$ that are perpendicular and parallel, respectively, to the shock, and similarly for the downstream flow vector, $\mathbf{q}_1 = \mathbf{q}_{1n} + \mathbf{q}_{1t}$. In this way one can unambiguously define the shock direction to be the same direction as the parallel vector components $\mathbf{q}_{0t} = \mathbf{q}_{1t}$. By this means it may be said that a wave arrives at a shock intersection point (i.e., node) R if the vector components $\mathbf{q}_{0t} = \mathbf{q}_{1t}$ point towards R, but the wave leaves R if $\mathbf{q}_{0t} = \mathbf{q}_{1t}$ point away from the it. (Our definition of the term arrives is equivalent to the definition of the term incoming used by Glimm et al. in [19]). Evidently a refracting shock can only arrive at a node R on an interface if its wave angle α with respect to the undisturbed interface m_u is acute, $\alpha < \pi/2$. For example, compare Fig. 8 where n arrives and t leaves R, with Fig. 11 where t arrives and s leaves R.

4.2 Wave direction and the principle of shock reciprocity

Consider two materials $\mathcal{M}_i$ and $\mathcal{M}_t$, each with a convex equation of state, which are initially in contact along a plane surface and in equilibrium under uniform compressive pressure. Now suppose a shock i, with shock strength $\xi_i \equiv P_0/P_1$, is started in the incident material $\mathcal{M}_i$ at a predetermined angle of incidence α_i, where α_i is chosen so that $\sin^2 \alpha_i = x$ and x is a solution of (16), so the resulting refraction will be a regular shock pair system. When the incident shock i strikes the undisturbed material interface m_u it refracts into a transmitted shock t with refraction angle α_t and also deflects the undisturbed interface by an angle δ down and away from itself. Note that this in the same direction as the wave direction of the incident shock (e.g., see Fig. 4). The three angles α_i, α_t and δ define the geometry of the regular shock pair system. Furthermore, note that the angle θ at R between the undisturbed material interface m_u and the disturbed material interface m_d measured in the incident material $\mathcal{M}_i$ or, equivalently, on the side of the interface with the incident shock i, is $\theta \equiv \pi + \delta > \pi$ radians.

The shock pair system is now in the self-similar configuration shown in Fig. 4.[3] Taking coordinates fixed with respect to the refraction node R, let $\mathbf{q}_0$ denote the velocity approaching R (i.e., $-\mathbf{q}_0$ is the velocity of R in the laboratory frame). The vector component of $\mathbf{q}_0$ parallel to the i-shock points towards R, so the i-shock arrives at R, while the analogous component for the t-shock points away from R, so the t-shock leaves R as shown in Fig. 4.

Now consider the reciprocal refraction, which we denote by i', t', $\alpha_{i'}$ and $\alpha_{t'}$. In the reciprocal refraction the two materials are exchanged, so the original transmission material $\mathcal{M}_t$ is now the new incident material $\mathcal{M}_{i'}$ and vice versa. The polar diagram does not change under this exchange, so both shocks have the same inverse incident shock strength $\xi_{i'} = \xi_i$ and the same deflection angle δ as before. An incident shock i' is now started in the new incident material $\mathcal{M}_{i'} = \mathcal{M}_t$ at the angle of incidence $\alpha_{i'} = \alpha_t$ with shock strength $\xi_{i'} = \xi_i$ (Fig. 14). In a neighborhood of the refraction node R the

---

[3] One can instead consider the system shown in Fig. 4, but without the bottom boundary, so the i and t shocks and the undisturbed and disturbed material interfaces m_u, m_d are rays that originate at R and extend to infinity in each of their respective directions.
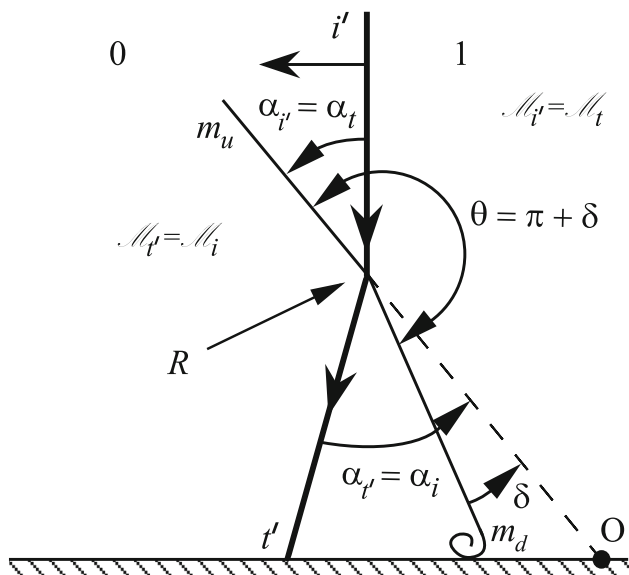
Fig. 14 Regular-shock-pair refraction (RSP) ($i'-t'$) that is reciprocal to the RSP in Fig. 4; the materials $\mathcal{M}_i$, $\mathcal{M}_t$ and the angles α_i, α_t and δ are the same as in Fig. 4; note that the angle θ is measured in radians

Fig. 15 Comparison of the approximate theory $\sin\alpha_i \approx U_i/U_m$ to experimental and numerical data; U_i is the speed of the incident shock i; U_m is the speed of the node R along the undisturbed material interface; *square, triangle, circle,* experimental, computational and approximate theory data points, respectively

geometry of the reciprocal system is identical to the original system except for one detail. The angle between the new incident and transmitted shocks i' and t' is the same as the angle between the original incident and transmitted shocks i and t, and the deflection angle δ is the same. However, in the reciprocal system the disturbed material interface m_d is downstream of the new incident shock i', which has angle of incidence $\alpha_{i'} = \alpha_t$, whereas in the original system the disturbed material interface m_d is downstream of the original incident shock i, which has angle of incidence α_i (Fig. 4), where, in general, $\alpha_i \neq \alpha_t = \alpha_{i'}$. Thus, in general, a photograph of a regular shock pair system and its reciprocal system would not be geometrically identical. This difference allows us to identify which of the two shocks in the system is the incident shock. Namely, the incident shock i (or i') is the shock on the side of the interface where the angle between the undisturbed, m_u, and the disturbed, m_d, material interfaces is $\theta = \pi + \delta > \pi$ radians as shown in Fig. 14. Inspection of the diagram in Fig. 14 of the system that is reciprocal to the system in Fig. 4 now reveals that the new incident shock i' arrives at R and the new transmitted shock t' leaves R.

From equation (3) we have $\sin\alpha_i = \eta \sin\alpha_t$, where η is the refractive index defined in (2). Exchanging the materials changes η to $\eta' = 1/\eta$ and hence, $\eta' \sin\alpha_i = \sin\alpha_t$. But the t-shock is now the new i-shock, namely i', and vice versa; so in exchanging the subscripts we recover equation (3) for the reciprocal system $\sin\alpha_{i'} = \eta' \sin\alpha_{t'}$. Furthermore, since $\eta < 1$ implies $\eta' = 1/\eta > 1$, if the original system is a slow–fast refraction, then the reciprocal system must be fast–slow refraction and vice versa. More formally, we have the following.
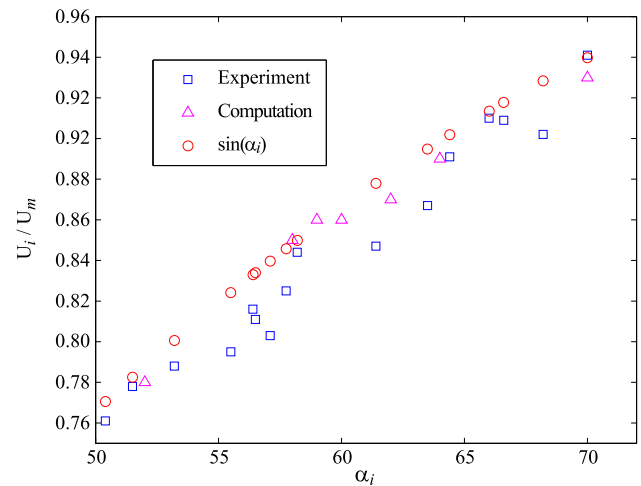
The principle of shock reciprocity Suppose that two materials, each with a convex equation of state, initially meet at a plane boundary and are everywhere under uniform compression. Then, if the two materials are interchanged, the polar diagram of a regular shock pair refraction, the angle between the two shocks, and the streamline deflection angle will be invariant. However, the two rays emanating from the refraction node R, which comprise the disturbed and undisturbed material interfaces in the original system, are reflected through R in the reciprocal system in such a way that the angle between the undisturbed and disturbed material interface, as measured in the incident material, is always $\theta = \pi + \delta > \pi$ radians. This is equivalent to the requirement that the incident shock is always the one that arrives at R.

Finally, both the refraction law (1) and the equality of impedance condition (11) are symmetrical for reciprocal shock pairs. It is concluded that the principal of shock reciprocity can be applied to regular shock pair systems provided we are always careful to identify the incident shock as the one that arrives at the refraction node R on the interface.

5 The experiments

The schlieren photographs and experimental data presented here were obtained from Abd-el-Fattah and Henderson [5]. We made additional measurements from their schlieren photographs, so the data presented in Figs. 15, 16, 17 and 18 has not been previously published. The experiments were done by setting up a delicate polymer membrane, with an areal density of about $5 \times 10^{-6}\,\mathrm{g\,cm^{-2}}$, in a shock tube. Then
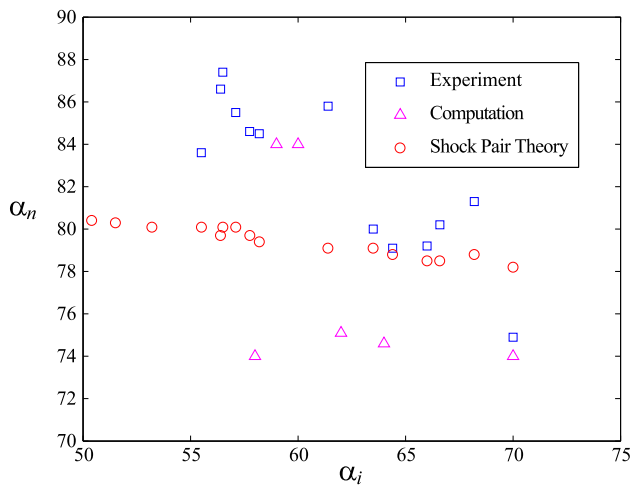
Fig. 16 Comparison of the shock pair theory to experimental and numerical data for α_n, the wave angle for the Mach shock n at R; *square*, *triangle*, *circle*, experimental, computational and shock pair theory data points, respectively
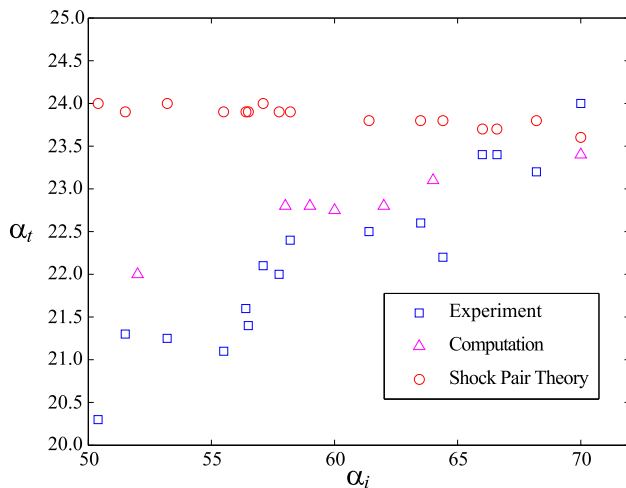

Fig. 17 Comparison of the shock pair theory to experimental and numerical data for α_t, the wave angle of the transmitted shock t at R; *square*, *triangle*, *circle*, experimental, computational and shock pair theory data points, respectively
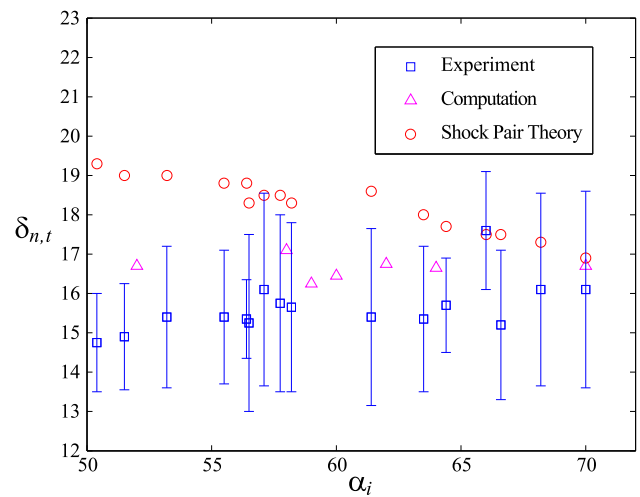

Fig. 18 Comparison of the shock pair theory to experimental and numerical data for the streamline deflection angles $\delta_{n,t}$, these are the same as the deflection angle δ of the material interface at R; *square*, *triangle*, *circle*, experimental, computational and shock pair theory data points, respectively; NB the *vertical lines* are *not error bars*, but are the measured angular width of the disturbed interface due to the gas mixing; e.g., see Fig. 11

air was introduced on one side of it and SF_6 on the other. The membrane defined the boundary between the gases as a plane surface. A plane shock wave was initiated in the air and arranged to strike the membrane (interface) at a predetermined angle of incidence α_i. The shock shattered the membrane and refracted as it entered the SF_6. This refraction is fast–slow because $\eta > 1$. A detailed description of the experimental apparatus and its operation may be found in [6], while a detailed description of the experiments from which the data presented here was obtained may be found in [5].

Some data with ξ_i held constant at $\xi_i = 0.25$ are presented in Figs. 15, 16, 17 and 18. These are for the MRR

type of refraction, a diagram of which is depicted in Fig. 8. A schlieren photograph of a MRR refraction appears in Fig. 10 and an enlargement of this photograph about the Mach stem appears in 11. In this system the shock pair is an $n - t$ shock pair in which the Mach shock n refracts and forms t. For all of these experiments the flow downstream of, and relative to, n is subsonic, while the flow downstream of, and relative to, t is supersonic.

6 The computations

6.1 The numerical method

In this work we used a second-order accurate finite difference method on a square grid (i.e., $\Delta x = \Delta y$) covering a rectangular, two-dimensional domain to approximate solutions of the time-dependent compressible Euler equations in which two gases are present. The boundary conditions consisted of reflecting boundary conditions on the left, top and bottom sides of the computational domain and inflow boundary conditions on the right-hand side of the domain; i.e., boundary cells on the right-hand side of the computational domain were set to the post-shock state for the incident shock i.

The basis of our numerical method is the numerical integration of the compressible Euler equations for a single gas with an operator split version of a second-order accurate Godunov method of the type originally proposed in [25,26] and [27]. This methodology is second-order accurate in regions of smooth flow and captures shocks with a min-

imum of numerical overshoot and dissipation. This second-order Godunov methodology for a single gas has been used extensively to compute unsteady shock reflections in gases and has a demonstrated ability to resolve complex interactions of waves and discontinuities that is in excellent agreement with experiment; e.g., see [28].

Our approach to modeling grid cells that contain more than one gas is based on an (unpublished) algorithm for modeling two gases in a single grid cell originally proposed by Colella, Glaz, Ferguson and Puckett. Although this algorithm is unpublished, it is a straightforward matter to modify the algorithm described in [29] for modeling cells that contain more than one material, each of which obeys a Mie–Grüneisen equation of state with a linear Hugoniot, to obtain the algorithm we used here for modeling cells that contain two perfect gases; one simply replaces the Mie–Grüneisen equation of state for each material with the ideal gas equation of state for each gas.

In our numerical method the interface between each gas is tracked using the "Least squares volume-of-fluid interface reconstruction algorithm" coupled to an operator split advection algorithm as described in [30]. In grid cells that contain two gases the equations of motion for a single gas are supplemented with evolution equations for the volume fraction, total energy and mass density of each gas. The resulting system of conservation laws is of hyperbolic type, and thus can be solved using a straightforward extension of the underlying second-order accurate Godunov method for a single gas. This formulation of the equations of motion accounts for the thermodynamic properties of each gas separately, while modeling the pressure and velocity in each grid cell, including those that contain more than one gas, as single-valued quantities. In particular, given a single uniform pressure acting on a grid cell containing two gases, this algorithm will correctly account for the compression or expansion that each gas undergoes as a result of that pressure.

We coupled this algorithm for approximating the solution of the compressible Euler equations with two gases to the adaptive mesh refinement algorithm described in [31]. In [2] we used this numerical method to model the wave interactions that occur when a shock wave strikes a slow–fast gas interface. Our results are in excellent agreement with the slow–fast shock refraction experiments reported in [6,7] and [17].

A detailed description of all aspects of the numerical method we used in the work described here may be found in [29]; the only difference being that in the work described here we used an ideal gas equation of state while in [29] the authors used a Mie–Grüneisen equation of state with a linear Hugoniot. However, as mentioned above, it is a straightforward procedure to covert the algorithm described in [29] into one in which the computational grid cells contain one or two gases, each of which obeys an ideal gas equation of state.

Table 1 Gas properties used in the computations

Gas	Air	CO_2	CH_4	SF_6
γ	1.4	1.288	1.303	1.093
μ	28.966	44.01	16.04	146.0544

6.1.1 Self-similar solutions of the compressible euler equations

Note that in Fig. 10 the t-shock undergoes a local Mach reflection at the bottom boundary and the reflected shock associated with this Mach reflection deflects the gas disturbed gas interface to the right, in a region close to the bottom boundary. In Samtaney and Pullin [32] and Samtaney [33] the authors introduce a numerical method for approximating solutions of the (steady) self-similar compressible Euler equations and use it to study the instability and subsequent roll-up of the gas interface in a fast–slow refraction at a density jump in a perfect gas (air). This is analogous to the experiment shown in Fig. 10. Their computations appear to correctly resolve the Mach reflection of the t-shock at the bottom boundary and the subsequent deflection of the gas interface by the reflected shock. In references [32] and [33] the authors present an interesting study that addresses the question of how accurately a numerical method can compute the roll-up of the fluid interface. (An example of such a roll-up can be seen in the contour plot of $\log \rho$ in Fig. 25.)

6.2 Plan of the numerical work

Our computations were planned as though we were doing a series of experiments in a shock tube. For a particular sequence the values of α_i were selected to cover the phenomena of interest, while the other parameters (γ_i, γ_t, μ_i, μ_t, ξ_i), or equivalently, (a_{0i}, a_{0t}, ξ_i), or (η_a, ξ_i) were held constant. The gas properties we used in our computations are listed in Table 1.

We non-dimensionalized the problem and computed the numerical results shown in Figs. 24 and 25 on a domain of (non-dimensional) size 1.00×0.72. We computed all of the other numerical results (i.e., those shown in Figs. 19, 20, 21, 22 and 23 and Figs. 26, 27) on a domain of size 1.12×0.72.

Our block structured adaptive mesh refinement algorithm starts with a uniform 'level 0' grid covering the entire domain and then automatically places blocks of finer grids in regions of the computed flow field that satisfy certain predefined grid refinement criteria. In our computations the level 0 grid had a (non-dimensional) value of $\Delta x^0 = \Delta y^0 = 0.01$, where the superscript '0' indicates that these are the values for the level 0 grid. In other words, the level 0 grid on the 1.00×0.72 domains consisted of 100×72 square cells and the level 0
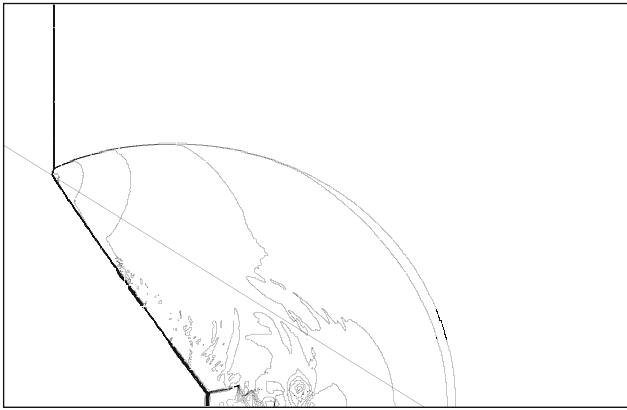
Fig. 19 Contour plot of log P for a MRR in Air/SF$_6$ with $\xi_i = 0.25$ and $\alpha_i = 58°$; this is a computation of the experiment shown in Fig. 10

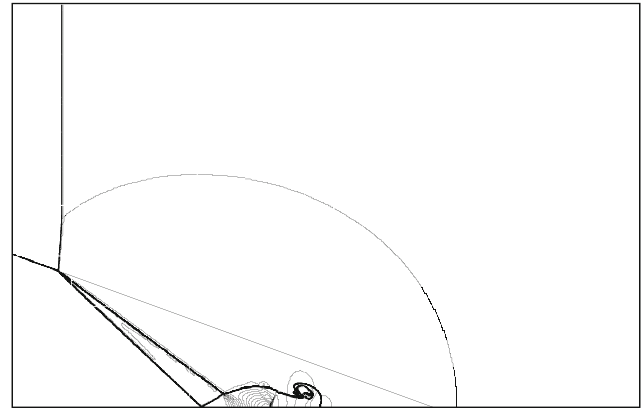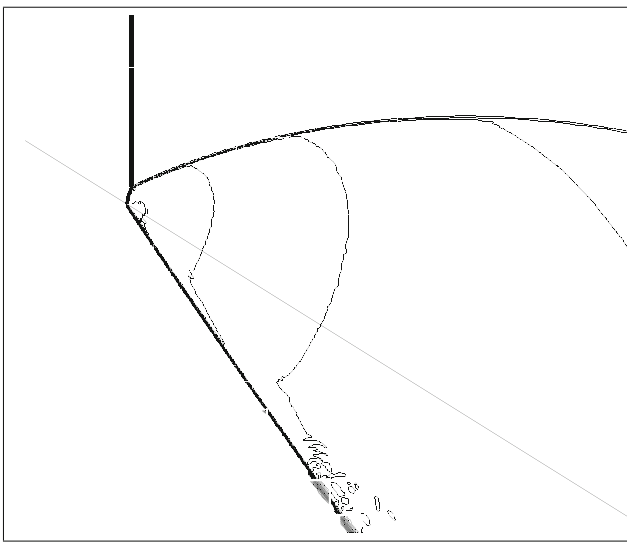**Fig. 21** Contour plot of log ρ for an ISP in Air/SF$_6$ with $\xi_i = 0.25$ and $\alpha_i = 70°$

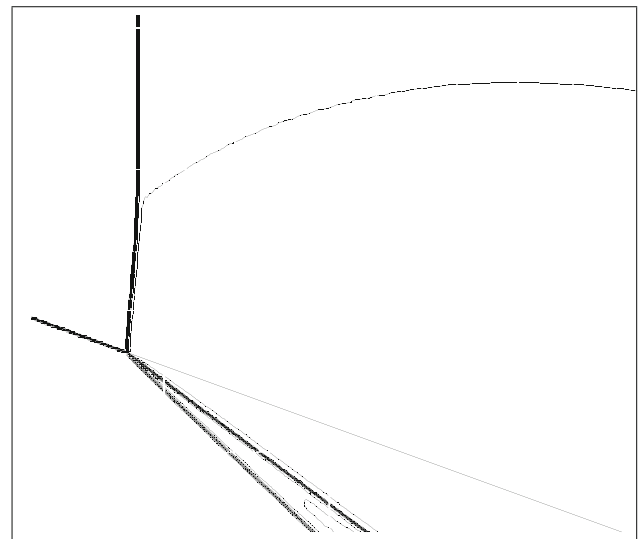**Fig. 20** Enlargement of Fig. 19 about the node R; compare with Fig 11

Fig. 22 Enlargement of Fig. 21 about the refraction node R

Fig. 23 Contour plot of log P for a RSP in Air/SF$_6$ with $\xi_i = 0.25$ and $\alpha_i = 77.65°$, the angle at which $\alpha_i = \alpha_p$; note there is no reflected wave

grid on the 1.12×0.72 domains consisted of 112×72 square cells.

The number of levels of refined grids and the amount by which they are refined from the level 0 grid are predefined computational parameters. The algorithm that determines when to refine a particular region of the grid is designed to automatically place finer grids in 'regions of interest', such as regions containing a portion of a shock wave or a portion of the gas interface. In particular, this algorithm has the property that the gas interface and all shock waves will be covered with blocks of the finest grid.

In computing all of the numerical results shown here we set the grid refinement parameters so there were at most two levels of grid refinement, each with a refinement factor of four. Thus, in addition to the level 0 grid some regions of the flow field were covered with blocks of a level 1 grid with $\Delta x^1 = \Delta x^0/4 = 0.0025$ and, additionally, some of the
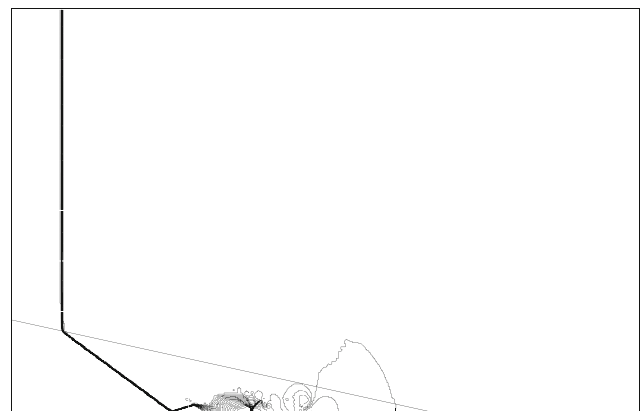
regions of the flow field covered by the level 1 grid were also covered with blocks of level 2 grids with $\Delta x^2 = \Delta x^1/4 = 0.000625$. So, for example, if one of the 1.00×0.72 domains
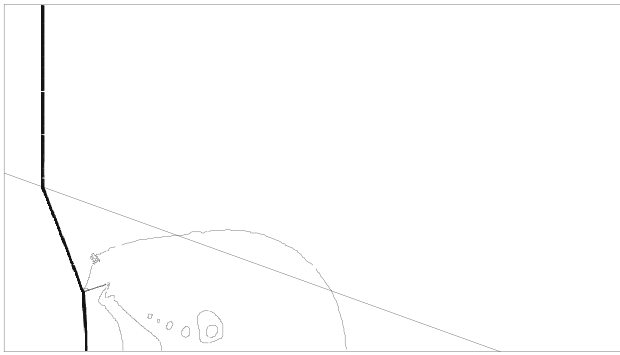
Fig. 24 Contour plot of log P for a RSP in Air/CO_2 with $\xi_i = 0.10$ and $\alpha_i = 70.2135°$, the angle at which $\alpha_i = \alpha_p$; note there is no reflected wave
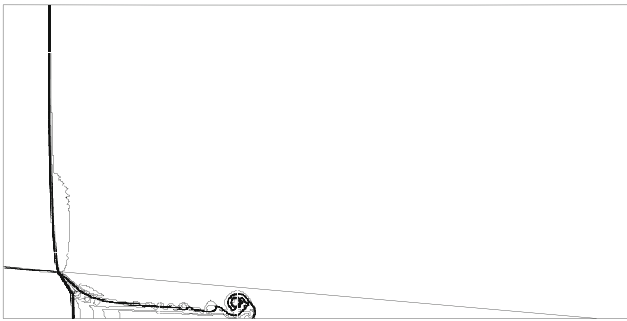

Fig. 25 Contour plot of log ρ for an ISP in Air/CO_2 with $\xi_i = 0.10$ and $\alpha_i = 85°$

Fig. 26 Contour plot of log ρ for a PCMR in Air/CH_4 with $\xi_i = 0.30$ and $\alpha_i = 55°$
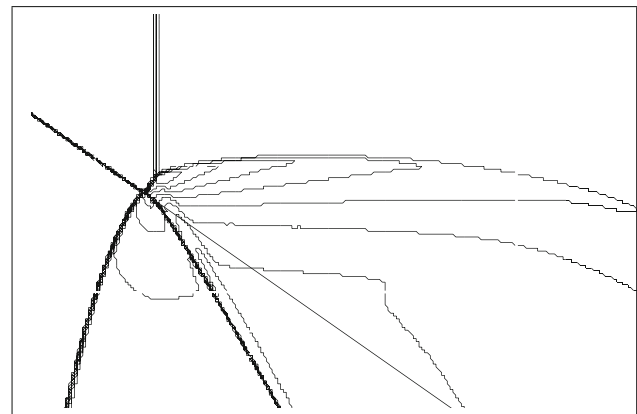
Fig. 27 Enlargement of the PCMR in Fig. 26 about the node R

had been uniformly covered with cells at the finest level of grid refinement, it would have been covered with $1,600 \times 1,152$ square grid cells.

We chose these values for the input parameters that controlled the formation of the computational grid so that further refinement of the grid did not change the wave angles and other features of the refracting wave systems in any way we could measure. We also checked our computational results by computing each of the problems with a uniform square grid at the finest level of refinement (i.e., with $\Delta x = \Delta y = 0.000625$) and found no measurable difference in the wave angles and other features of the refracting wave systems that appear in the contour plots in Figs. 19, 20, 21, 22, 23, 24, 25, 26 and 27.

We employed two-grid refinement criteria. First, all 'multifluid' cells (i.e., cells that contained both gases) were refined to the maximum extent. The second grid refinement criterion was designed to reduce the local truncation error in the computed values of the density ρ, where the local truncation error is estimated using a method based on Richardson extrapolation. Details of the error estimation algorithm may be found in [31] and [29].

Note that this algorithm is adaptive in the sense that as the flow field evolves in time it detects the location of both shock waves and the gas interface, even if they are moving,

and automatically places blocks of the level 1 and level 2 grids in a neighborhood of these features and removes blocks of these grids if these features leave the region (i.e., if the grid refinement criteria mentioned above ceases to hold). For a more detailed account of the block structured adaptive mesh refinement algorithm see references [31] and [29]. Each of these references contain figures showing the automatic placement of the refined block grid structure over regions of the computed flow field with moving shock waves and, in [29], the interface between two materials.

The vertical lines in Fig. 18 accompanying the experimental data for $\delta_t = \delta_n$ indicate the measured angular width of the disturbed gas interface (e.g., see Figs. 10, 11), they are not error bars.

7 Discussion

7.1 Comparison with experiment

In Figs. 15, 16, 17 and 18 we compare experimental data and data we obtained from our numerical computations to

data we calculated with the regular shock pair theory. As we mentioned in the last paragraph of Sect. 5, the experimental data is from experiments in which the refraction was of the MRR type, a diagram of which appears in Fig. 8. With regards to the accuracy of the experimental data, the speed U_m of the $n - t$ node along the undisturbed gas interface and the angle of incidence α_i could both be measured to about 3 significant figures from the schlieren photographs of the experiments. We consider the U_i/U_m versus α_i data shown in Fig. 15 to be our most accurate and reliable results. The other experimental data presented here, which are all angles, are less accurate and are typically no better than $\pm 2°$. An exception is the α_n[4] versus α_i data shown in Fig. 16, which was difficult to measure accurately for all but the largest values of α_i because of the relatively short length of the n-shock.

The numerical data[5] is in excellent agreement with the experimental data for U_i/U_m in Fig. 15, and in agreement with the experimental angle data in Figs. 17 and 18 granted the uncertainties in the measurements taken from the experiments and the numerics. In general, for $\alpha_i < 65°$ the numerical data for α_n shown in Fig. 16 does not agree well with the experimental data. We attribute this to the difficulty we had in measuring α_n for $\alpha_i < 65°$ in both the experiments and the computations. This difficulty is due to the fact that for $\alpha_i < 65°$ the n-shock is quite short; significantly shorter than the t-shock and both the undisturbed and disturbed gas interfaces. As a consequence, for $\alpha_i < 65°$ we were unable to establish a line tangent to n at R that was accurate to within $\pm 2°$. We consider the α_n versus α_i data for $\alpha_i < 65°$ to be our most unreliable data.

It is important to note that the strength of the $n - t$ shock pair is not known from the experiments and therefore, the shock pair theory as given in equations (16) and (18) cannot be used. Furthermore, in the derivation of the shock pair theory [i.e., equations (16)–(18)] we assume that the refraction is a regular shock pair, which, in the case of each of the experiments for which data is presented in Figs. 16, 17 and 18, is not necessarily true. In short, the data represented as circles in Figs. 16, 17 and 18 and labeled 'Shock pair theory' is based on our calculation of the angles α_n, α_t and $\delta_{n,t}$ versus α_i under the (possibly untrue) assumption the refraction is a regular shock pair. We calculated this data in the following manner.

Given the values of the sound speeds a_{0i} and a_{0t} ahead of the incident and transmitted shocks and the value of the

inverse incident shock strength $\xi_i = 0.25$, each of which is known a priori, together with the measured value of the speed U_m of the $n - t$ node from each experiment, we calculated the undisturbed free stream shock Mach numbers upstream of, and relative to the n and t shocks: $M_{0n} = U_m/a_{0i}$ and $M_{0t} = U_m/a_{0t}$ (e.g., see Fig. 2). Using M_{0n} and the ratio of specific heats γ_i for the incident gas (air) we then formed the shock polar for the n shock. Similarly, we used M_{0t} and γ_t to form the shock polar for the t shock in the transmitted gas (SF_6). Given the shock polars for the n and t shocks we used Newton's method to find their intersection $(\delta, \ln(P_1/P_0))$. At this point of intersection equation (13) holds, $P_{1n} = P_{1t}$, and similarly for the streamline deflection angle $\delta_n = \delta_t$ across the n and t shocks. We plot this latter quantity against α_i in Fig. 18. Furthermore, now that we know P_{1n} and P_{1t}, we can determine the shock speeds U_n and U_t for the n and t shocks. These quantities, together with U_m, give us α_n and α_t from the identities $\sin \alpha_n = U_n/U_m$ and $\sin \alpha_t = U_t/U_m$. We plot α_n and α_t against α_i in Figs. 16 and 17, respectively. Actually, using the refraction law (1) one obtains the very good approximation $U_n/U_m \approx \sin \alpha_i$, as shown by the circles in Fig. 15. This equation becomes strictly correct if the MRR transits to a regular refraction: MRR $\rightarrow$ RRR, in which case the normal shock n disappears and the incident shock i meets the transmitted shock t at the node R.

Our reason for presenting the 'Shock Pair Theory' data in Figs. 16, 17 and 18, calculated in the manner just described, is to show the agreement between the data from the regular shock pair theory and the experimental and computational data increases as α_i increases, until there is complete agreement between the regular shock pair theory and our computations at $\alpha_i = \alpha_p = 77.65°$. This is the angle at which the regular shock pair theory predicts there will be a regular shock pair for the Air/SF_6 gas combination with $\xi_i = 0.25$. This prediction is confirmed by the contour plot in Fig. 23. Unfortunately, we have no experimental data for $\alpha_i = 77.65°$. This is the reason $\alpha_i = 70°$ is the upper limit for the horizontal axis in Figs. 15, 16, 17 and 18.

In summary, for $\alpha_i < 77.65°$ there are discrepancies between the experimental data and the data calculated from the regular shock pair theory as described above. Thus, although the n and t shocks form a shock pair for $\alpha_i < 77.65°$, this shock pair system is not regular (uniform) and therefore it must instead be an irregular shock pair system (non-uniform). We shall present numerical evidence to support this hypothesis in Sect. 7.2. However, before presenting this evidence, we first explore the implications of our observations concerning the data in Figs. 16, 17 and 18 by briefly re-examining the shock pair theory.

The shock pair theory for the refraction of the $i - t$, $n - t$, and $t - s$ pairs involves both the refraction law (1) and the equality of impedance condition (11), where the subscript i is replaced by n for the $n - t$ pair and, sim-

---

[4] The Mach shock wave angle α_n and the side shock wave angle α_s are measured with respect to the upstream undisturbed interface m_u; i.e., in the same way the incident shock wave angle α_i is measured (Fig. 1).

[5] Throughout this article the words 'numerical', 'computation' and their variants always refer to results obtained from computations made with the numerical method described in Sect. 6.1, while the word 'calculate' and its variants always refer to results obtained 'by hand' or with a calculator.

ilarly, the subscripts i and t are replaced by t and s for the $t-s$ pair. The refraction law must be correct, otherwise one shock would move along the interface faster than the other and the system would disintegrate. The equality of impedance condition requires the von Neumann boundary conditions to be satisfied everywhere along the interface; that is, the component of the velocity of both materials normal to the interface must be equal at any point on it, and so also must be the pressure. The validity of these conditions has been well established by innumerable experiments, not only in the references cited but in many other papers on Mach reflections and shock interactions. The von Neumann conditions can therefore also be accepted with confidence. Now the equality of impedance condition (11) is obtained essentially by taking the ratio of these conditions [1], so it must also be correct. However, the regular shock pair theory also uses a third equation, namely (13), and both experiments and computations indicate it is not correct in a neighborhood of the refraction node R in the event subsonic non-uniformities are present. Hence, the refraction becomes irregular.

To summarize, consider an irregular shock pair, say a $t-s$ pair. At the refraction node R of the $t-s$ pair their respective impedances must be equal $Z_t = Z_s$ for the reasons stated above. However, as one moves away from R along either the t or s-shock there are subsonic non-uniformities in the pressure field downstream of each shock and hence, also in the velocity field, causing the impedances Z_t and Z_s to differ from one another in an immediate neighborhood of R. The changes in the pressure in an immediate neighborhood of R downstream from each shock also cause the shock to curve as one moves away from R. This is particularly evident in the computation of the PCMR in Air/CH4 in Figs. 26 and 27. Some additional numerical evidence for uniform and non-uniform flows will be presented in the next section.

However, before proceeding we would like to emphasize that one can apply the regular shock pair theory without a priori knowledge of a system parameter that must be obtained from experiment or computation. The reason it was necessary for us to use the experimental value of the speed U_m to calculate α_n, α_t and $\delta = \delta_n = \delta_t$ from the regular shock pair theory as described above was because we wanted to compare the theory with experimental data to determine if the $n-t$ shock pairs were regular. In general, however, one can use the regular shock pair theory to predict the angle $\alpha_i = \alpha_p$ at which a regular shock pair will occur when a planar shock with incident shock strength ξ_i refracts at a planar interface between two materials. For example, in [3] we used the regular shock pair theory in this manner to study anomalous refraction at an Air / CO_2 gas interface. All of our computations, including the ones shown in Figs. 23 and 24, have agreed with the predictions made by the regular shock pair theory when we have used it this way.

7.2 The computational results

7.2.1 Supersonic–subsonic

In Figs. 19, 20, 21, 22 and 23 we present computational results[6] for the gas combination Air / SF$_6$ with $\xi_i = 0.25$ and α_i in the range $58° \leq \alpha_i \leq \alpha_p = 77.65°$. In Fig. 19 there are closely spaced pressure contours near the $n-t$ node; this is clearer in the enlargement in Fig. 20. Therefore, we conclude that the flow is non-uniform and the $n-t$ refraction is irregular. Figs. 16, 17 and 18 show that the regular shock pair theory differs significantly from experiment for $\alpha_i = 58°$. However, the computational wave angle data in Figs. 17 and 18, which make no assumption about regularity (uniformity), agrees to within $\pm 2°$ with the experimental wave angle data at $\alpha_i = 58°$, which is within the accuracy with which the experimental and computational wave angle data in these figures could be measured. One can also see the degree to which the computation agrees with the experiment by comparing the schlieren photographs in Figs. 10 and 11 with the contour plots in Figs. 19 and 20.

As we continuously increase α_i it eventually approaches the regular shock pair condition at $\alpha_i = \alpha_p = 77.65°$, where $Z_t = Z_i$. During this process the contours become increasingly sparse near R and the local flow correspondingly more uniform. For example, compare Figs. 21 and 22 where $\alpha_i = 70°$ with Figs. 19 and 20. Inspection of Figs. 15, 16, 17 and 18 shows the agreement between the RSP theory and experimental data increases steadily with increasing α_i. At $\alpha_i = 70°$ the values for U_i/U_m from the regular shock pair theory and the experimental data are indistinguishable in Fig. 15 while the angle data in Figs. 17 and 18 is within $\pm 2°$, which is the limit of the accuracy with which the computational and experimental wave angle data could be measured. However, both the data for α_n in Fig. 16 (which for $\alpha_i = 70°$ can be measured as accurately as the other wave angle data) and the contour plots in Figs. 21 and 22 show the refraction at $\alpha_i = 70°$ is not yet a regular shock pair. We have no experimental data at the regular condition $\alpha_i = \alpha_p = 77.65°$. However, the regular theory is in excellent agreement with the numerical results at this condition as shown in Fig. 23. Physically the reflected shock has now vanished $Z_r = 0$ and the i and n shocks have become indistinguishable, $Z_t = Z_n = Z_i$.

By comparing the regular shock pair theory, the numerical and the experimental results we conclude that both regular (uniform) and irregular (non-uniform) shock pair refractions exist. In particular, the irregular refractions include rapid

---

[6] In each of Figs. 19, 20, 21, 22, 23, 24, 25, 26 and 27 we have drawn a straight line at the angle α_i to the vertical in order to indicate the initial position of the gas interface. This line is in the same location as the edge of the wire frame that holds the thin polymer membrane that initially separates the two gases in the experiments, and is visible in Figs. 10 and 11.

changes in the pressure in a subsonic flow field about the refraction node. If the node becomes a source/sink of contours, then the non-uniformity becomes a subsonic pressure discontinuity at that point.

Other examples are presented in Figs. 24 and 25; these are for Air/CO_2 with $\xi_i = 0.10$. In Fig. 24 $\alpha_i = \alpha_p = 70.2135°$ and the refraction is regular. The i- and t-shocks are perfectly straight in a neighborhood of their intersection at the refraction node R on the gas interface and there are no reflected waves. Hence, the regular shock pair theory is again in excellent agreement with the numerical results. In Fig. 25 $\alpha_i = 85°$ and the refraction is irregular. In this case the i-shock is curved in a neighborhood of its intersection with the t-shock and there is a reflected wave in a neighborhood this intersection. Consequently, the regular shock pair theory is not in good agreement with the numerical results. Since the refraction is irregular this is to be expected. For all of these examples the flow is subsonic downstream of the Mach shock n, and supersonic downstream of the transmitted shock t.

7.2.2 Shock pairs in PCMR systems

Two interferograms of PreCursor-Mach-refraction (PCMR) systems for the Air/CH_4 gas combination with $\xi_i = 0.3$ were published by Jahn; namely, Fig. 14c, Plate 6 and Fig. 18, Plate 12 of [17]. Our numerical results for the Air/CH_4 gas combination with $\xi_i = 0.3$ and $\alpha_i = 55°$ are presented in Figs. 26 and 27. The non-uniformity about the $(t - s)$ node is clear. Superficially the wave system resembles the Mach-reflection–refraction (MRR) shown in Fig. 10. However, there is the important difference that the t-shock is now forward leaning, $\alpha_t > \pi/2$, so it arrives at the refraction node R rather than leaves it. The t-shock transmits a wave called the side shock s back into the initial material and s leaves the node R. Thus $t - s$ form a precursor pair of shocks in which t is driven from its rear by disturbances that arise in the initial material, such as for example by the bursting of a shock tube diaphragm. Subsequently s interacts with i to produce the Mach shock n and the reflected shock r. The shocks n and s meet at the point N where they are both normal shocks. The r shock leaves the triple shock node (i, n, r) in the usual way as shown in Fig. 11.

We have called system shown in Fig. 11 a PreCursor-Mach-refraction (PCMR). It is evident that a PCMR system is separated from an MRR system by the condition that n, s, and t are all perpendicular to the interface $\alpha_t = \alpha_s = \alpha_n = \pi/2$ and hence, $Z_t = \infty$. This means $x = 1$ in (16) and the coefficients of equations (17) and (18) satisfy

$$A_2 + A_1 + A_0 = 0,$$
$$B_2 + B_1 + B_0 = 0,$$

respectively.

In [2], we present detailed numerical and shock polar studies of different types of PCMR systems. This work includes schlieren photographs of several different $t - s$ shock pairs in PCMR systems from the experiments of Abd-el-Fattah and Henderson [7]. For example, we present an experiment (a schlieren photograph), color and contour plots from our numerical computations, and the polar diagram of a $t - s$ shock pair, which we refer to as a Twin-Mach-reflection refraction (TMR) in Figs. 8d, e, 9a–c and 10e of [2]. We refer the reader interested in PCMR systems to references [2,6,7], and [17].

8 Conclusions

We have presented experimental and computational evidence to support our claim that there are two distinct classes of shock pair refractions. A shock pair refraction may be either a regular-shock-pair refraction (RSP) or an irregular-shock-pair refraction (ISP). We have developed a theory for RSP systems for materials with convex equations of state and presented a method for classifying the different types of ISP systems.

In our theory for RSP refractions we assume the pressure jumps $P_{1i}/P_0 = P_{1t}/P_0$ and streamline deflection angles $\delta_i = \delta_t$ or, equivalently, the shock wave impedance across the incident i and transmitted t shocks are equal $Z_i = Z_t$. This will be true if the flow fields are uniform in a neighborhood of the refraction node R. We have derived an equation, namely, equation (16), one can use to predict the angle of incidence $\alpha_i = \alpha_p$ at which an RSP will occur. At this angle of incidence there will be no reflected wave at R, only the incident and transmitted shocks are there and hence, there will be total transmission of the incident shock into the transmission material.

Equation (16) depends only on the initial and receiving materials' equations of state, their initial (undisturbed) thermodynamic states, and the incident shock strength ξ_i. The only restriction on the initial and receiving materials is that the fundamental derivative $\mathcal{G}$ of each material must be positive, $\mathcal{G} > 0$. We show that an RSP is not robust and appears as a separating condition between regular or irregular refractions or as the limit of a continuum of ISP refractions. We have derived formulas for the coefficients of (16) for this most general case, and also for the specific case in which the two materials are perfect gases. We have presented computational results for this latter case, where the two materials are both perfect gases, that verifies (16) correctly predicts the value of $\alpha_i = \alpha_p$.

We also show an RSP obeys the *Principle of Shock Wave Reciprocity*, which is analogous to the Principle of Reciprocity in acoustics [4]. Namely, if the two materials are exchanged then the polar diagram, the angle between the two shocks and the deflection angle of the material interface

remain the same. In this event we have shown how to use the wave direction of each member of the shock pair to determine which is the incident and which is the transmitted shock.

An ISP will have at least one non-uniform flow field about the refraction node R; that is, there will be significant changes in the flow properties, such as the pressure, in every open neighborhood of R. The more rapid the changes the more severe will be the nonuniformity and in the most severe case the node will be a singular source/sink of contours that may correspond to a subsonic pressure discontinuity at the node.

We have also categorized irregular shock pair refractions according to whether the flow Mach number downstream and relative to each shock in the pair is either supersonic or subsonic, and presented experimental and computational evidence for the existence of these systems. In particular, we have identified two such systems, which we refer to as a Mach-reflection–refraction (MRR) and a PreCursor-Mach-refraction (PCMR), and shown that equation (16) takes on a special form at the point of transition MRR $\rightleftharpoons$ PCMR between a MRR and a PCMR.

In future work, we plan to use the theory presented here, together with other ideas, to develop a more general theory to deal as fully as possible with the larger group of phenomena that comprise anomalous shock refraction.

References

1. Henderson, L.F.: On the refraction of shock waves. J. Fluid Mech. **198**, 365–386 (1989)
2. Henderson, L.F., Colella, P., Puckett, E.G.: On the refraction of shock waves at a slow–fast gas interface. J. Fluid Mech. **224**, 1–27 (1991)
3. Puckett, E.G., Henderson, L.F., Colella, P.: A general theory of anomalous refraction. In: Brun, R., Dumitrescu, L.Z. (eds.) Shock Waves @ Marseilles, vol. IV, pp. 139–144. Springer, New York (1995)
4. Kinsler, L.E., Frey, A.R., Coppens, A.B., Sanders, J.V.: Fundamentals of Acoustics, 4th edn. Wiley, London (1999)
5. Abd-el-Fattah, A.M., Henderson, L.F.: Shock waves at a fast–slow gas interface. J. Fluid Mech. **86**, 15–32 (1978)
6. Abd-el-Fattah, A.M., Henderson, L.F., Lozzi, A.: Precursor shock waves at a slow-fast gas interface. J. Fluid Mech. **76**, 157–176 (1976)
7. Abd-el-Fattah, A.M., Henderson, L.F.: Shock waves at a slow–fast gas interface. J. Fluid Mech. **89**, 79–95 (1978)
8. Courant, R., Friedrichs, K.O.: Supersonic Flow and Shock Waves. Springer, New York (1976)
9. Ames Research Staff: Equations, tables, and charts for compressible flow. Tech. Rep. 1135, Ames Aeronautical Laboratory, Moffett Field (1953)
10. Courant, R., Friedrichs, K.O.: Supersonic Flow and Shock Waves, Applied Mathematical Sciences, vol. 21. Springer, New York (1985)
11. Thompson, P.A.: Compressible Fluid Dynamics. McGraw-Hill, New York (1972)
12. Grove, J.W.: The interaction of shocks with fluid interfaces. Adv. Appl. Math. **10**, 201–227 (1989)
13. Grove, J.W., Menikoff, R.: Anomalous reflection of a shock wave at a fluid interface. Adv. Appl. Math. **219**, 313–336 (1990)
14. Lax, P.D.: Hyperbolic Systems of Conservation Laws and the Mathematical Theory of Shock Waves. SIAM, Philadelphia, PA (1973)
15. Zel'dovich, Y.B., Raizer, Y.P.: Physics of Shock Waves and High Temperature Hydrodynamic Phenomena, vol. I. Academic Press, New York (1966)
16. Henderson, L.F.: The refraction of a plane shock wave at a gas interface. J. Fluid Mech. **26**(3), 607–637 (1966)
17. Jahn, R.G.: The refraction of shock waves at a gaseous interface. J. Fluid Mech. **1**, 457–489 (1956)
18. Polacheck, H., Seeger, R.J.: Refraction of plane shock waves. Phys. Rev. **84**(5), 922–929 (1951)
19. Glimm, J.G., Klingenberg, C., McBryan, O., Plohr, B.J., Sharp, D.H., Yaniv, S.: Front tracking and two-dimensional Riemann problems. Adv. Appl. Math. **6**(3), 259–290 (1985)
20. von Neumann, J.: Oblique reflection of shock waves. In: Taub, A. (ed.) Collected Works, vol. 6. Pergamon Press, New York (1963)
21. Menikoff, R., Plohr, B.J.: The Riemann problem for fluid flow of real materials. Rev. Mod. Phys. **61**, 75–130 (1989)
22. Bethe, H.: The theory of shock waves for an arbitrary equation of state. Tech. rep., Clearing house for Federal Scientific and Technical Information, US Dept. of Commerce, Washington, DC (1942). Report No. PB-32189
23. Cramer, M.S., Sen, R.: Exact solutions for sonic shocks in van der Waals gases. Phys. Fluids A **30**, 377–385 (1987). doi:10.1063/1.866388
24. Thompson, P.A., Carafano, G., Kim, Y.G.: Shock waves and phase changes in a large-heat-capacity fluid emerging from a tube. J. Fluid Mech. **166**, 57–92 (1986)
25. Colella, P., Glaz, H.M.: Efficient solution algorithms for the Riemann problem for real gases. J. Comput. Phys. **59**, 264–289 (1985)
26. Colella, P., Woodward, P.: The piecewise-parabolic method (PPM) for gas-dynamical simulations. J. Comput. Phys. **54**, 174–201 (1984)
27. Colella, P.: A direct Eulerian MUSCL scheme for gas dynamics. SIAM J. Sci. Stat. Comput. **6**, 104–117 (1985)
28. Glaz, H.M., Colella, P., Glass, I.I., Deschambault, R.L.: A numerical study of oblique shock reflections with experimental comparisons. Proc. R. Soc. Lond. Ser. A **398**(1), 117–140 (1985). doi:10.1098/rspa.1985.0028
29. Miller, G.H., Puckett, E.G.: A high-order Godunov method for multiple condensed phases. J. Comput. Phys. **128**(1), 134–164 (1996)
30. Pilliod, J.E., Puckett, E.G.: Second-order accurate volume-of-fluid algorithms for tracking material interfaces. J. Comput. Phys. **199**(2), 465–502 (2004)
31. Berger, M.J., Colella, P.: Local adaptive mesh refinement for shock hydrodynamics. J. Comput. Phys. **82**(1), 64–84 (1989). doi:10.1016/0021-9991(89)90035-1
32. Samtaney, R., Pullin, D.I.: On initial-value and self-similar solutions of the compressible Euler equations. Phys. Fluids **8**(10), 2650–2655 (1996)
33. Samtaney, R.: Computational methods for self-similar solutions of the compressible Euler equations. J. Comput. Phys. **132**, 327–345 (1997)